Theoretical Notes

Note 367

July 9, 2002

On the Modeling and Representation of a Lossy Earth for Transient Electromagnetic Field Calculations

F. M. Tesche
EMConsultant
119 Miller Mountain Rd
Saluda, NC 28773
Fred@Tesche.com

Abstract

This report discusses the modeling of a lossy earth for NEMP coupling and assessment calculations. Measurements of the relative dielectric constant and electrical conductivity of the earth indicate that these quantities can vary significantly with frequency; they are not the simple constants that are often assumed in such calculations. Using several different representations of the frequency dependence of the measured earth parameters, calculations are performed to illustrate the typical frequency domain and transient behavior of EM fields above and in the earth, as well as the induced currents on an aboveground transmission line.

This work was sponsored by the Swiss NEMP Laboratory, under Defense Procurement Agency Contract 151-186.

Acknowledgement

I would like to acknowledge the support and interest in this project by my technical contract monitor, Dr. Armin Kälin, formerly of the Swiss NEMP Laboratory and presently at Meteolabor AG, in Wetzikon, Switzerland. In addition, thanks are due to Mr. Mike Messier of Metatech, Inc, and Dr. Kendall Casey of SRI International for providing some of their original source material, and for helpful discussions about various aspects of this report. Finally, thanks are due to Dr. Carl Baum, of the US Air Force Research Laboratory at Kirtland AFB, New Mexico, both for his interest in this subject, and for creating and maintaining this EM note series.

Contents

Figures

Tables

On the Modeling and Representation of a Lossy Earth for Transient Electromagnetic Field Calculations

1. Introduction

Many of the previous investigations into the effects of the nuclear electromagnetic pulse (NEMP) on electrical systems in the presence of the earth have used a highly simplified model for the electrical parameters of the soil. These usually involve modeling the earth as a lossy dielectric, having a frequency independent relative permittivity ε_r (dielectric constant) of about 10, a fixed electrical conductivity σ on the order of 0.001 to 0.1 s/m, and a relative magnetic permeability of μ_r of unity [1, 2, 3]. It is well known, however, that in a real earth the constitutive parameters σ, ε and μ can be functions of frequency, with rather large variations in their values [4].

The question naturally arises as to the level of error introduced into numerical simulations of HEMP system responses using the simplified earth parameters. Moreover, as the actual earth parameters may vary from point to point at a particular site and not be very well known, it is of interest to evaluate the sensitivity of a calculated response to variations in these parameters.

To help answer these questions, a study of the influence of these ground constitutive parameters has been conducted, and the results are discussed in this report. Because the relative magnetic permeability of the earth is usually close to unity in most cases, in this work we do not include this parameter as a variable, and we treat only variations in the parameters σ and ε.

In Section 2, a brief overview of past measurements and models for the earth's constitutive parameters is given. A key aspect of this work is insuring that the parameters satisfy the Kramer-Kronig relationships so as to provide causal responses in the time domain.

Section 3 discussed the effects of the earth parameter models on the EM responses that are typically encountered in a HEMP coupling problem. Variations of the earth propagation constant and wave impedance are studied for the various soil models, and the behavior of reflected and transmitted transient fields at the air-earth interface is displayed. In addition, the behavior of the induced current on an aboveground transmission line is calculated for these models.

Finally, in Section 4, a brief summary of the work and recommendations for future modeling activities are made.

2. Summary of Measured Earth Properties

Much of the past work on the understanding and representation of earth electrical parameters has been conducted for geophysical prospecting purposes [5, 6]. At low frequencies, the earth conductivity can be estimated in-situ by a four-point probe resistance measurement, used together with a suitable model relating the conductivity and the resistance. At higher frequencies, measurements of electromagnetic (EM) wave attenuation properties can be used to indirectly determine the material parameters.

Interest in this subject was renewed in the 1960's with the concern about NEMP and its effects on systems. Because the NEMP excitation is broad-band, the computational models for estimating system responses to this electrical stress had to be able to provide accurate results over a frequency range of several KHz to well over 100 MHz. As a result, several projects to better characterize the earth in this frequency range were started.

2.1 Measured Earth Parameters

2.1.1 Measurements by Scott

Using measurements of plane wave attenuation in an unbounded dielectric medium, Scott [7] discussed the results of an early project to determine the electrical properties of various soil simples from 100 Hz to 1 MHz. Tests of earth samples having different water content were conducted, and plots of the parameters σ, ε and μ were developed as a function of frequency and the percentage of water content. More important, however, was the fact that this reference provided a preliminary curve-fit expression for the parameters σ and ε for an arbitrary frequency and water content.

In a follow-on paper [8], refined curve-fit models for the earth parameters were provided on the basis of additional measurements obtained by the author and his colleagues. In this report Scott discussed the field and laboratory measurements, which were made to determine the electrical conductivity, dielectric constant, and magnetic permeability of rock and soil. The conductivity was determined by making field measurements of apparent resistivity at very low frequencies (0 to 20 Hz), and interpreting the true resistivity of layers at various depths by curve-matching methods. Interpreted resistivity values obtained in this manner were converted to corresponding conductivity values, which were *assumed* to be applicable at 100 Hz. Conductivity was estimated at higher frequencies (up to 1 MHz) by using statistical correlations of three parameters obtained from laboratory measurements of rock and soil samples: the electrical conductivity at 100 Hz, the frequency and the conductivity measured over the range 10 Hz to 1 MHz. The dielectric constant was estimated in a similar manner from field-derived conductivity values applicable at 100 Hz, and statistical correlations of three aforementioned laboratory measurement parameters

In this report, Scott suggests the following expressions for the relative *effective dielectric constant*[1] $\varepsilon_{eff}/\varepsilon_o$ and the *effective conductivity* σ_{eff}:

$$\frac{\varepsilon_{eff}}{\varepsilon_o} = 10^{\left[4.905+1.308\log(W)-0.971\log(f)+0.111\log^2(W)-0.168\log(f)\log(W)+0.059\log^2(f)\right]} \quad (1a)$$

$$\sigma_{eff} = 10^{\left[-0.604+1.64\log(W)-0.062\log(f)+0.062\log^2(W)-0.070\log(f)\log(W)+0.021\log^2(f)\right]}, \quad (1b)$$

where f is the frequency in the range 100 Hz to 1 MHz, and W is the water content of the soil in percent by volume. Figure 1 presents plots of $\varepsilon_{eff}/\varepsilon_o$ and σ_{eff}: for soil with water contents of 0.1% to 100%. Note that although the curve-fitting of the measured data was over the frequency range 100 Hz to 1 MHz, the data in Figure 1 have been extrapolated to 100 MHz for our use in fast pulse calculations for the HEMP environment.

[1] For a discussion of these effective earth parameters, how they are related to other possible representations of the earth, and how they enter into Maxwell's equations, consult Appendix A.

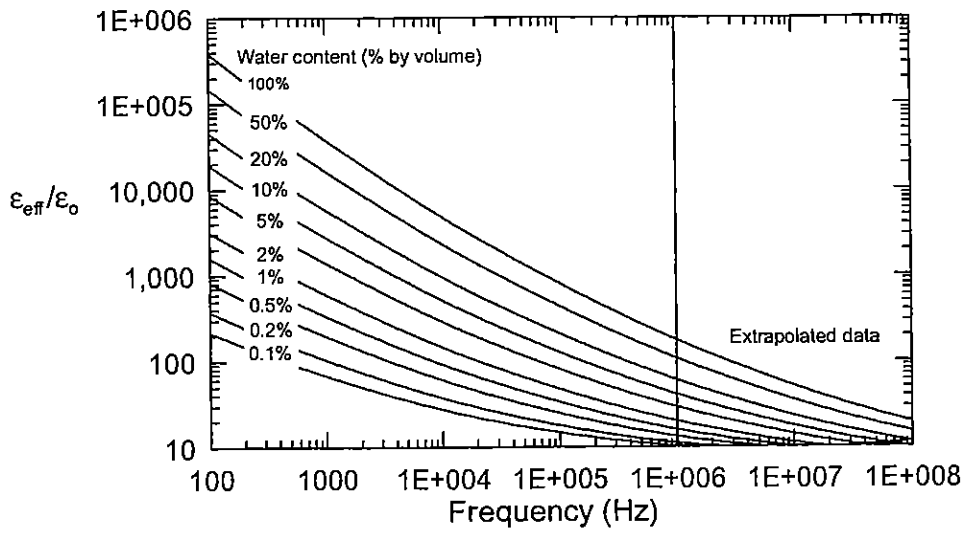

a. Relative effective dielectric constant

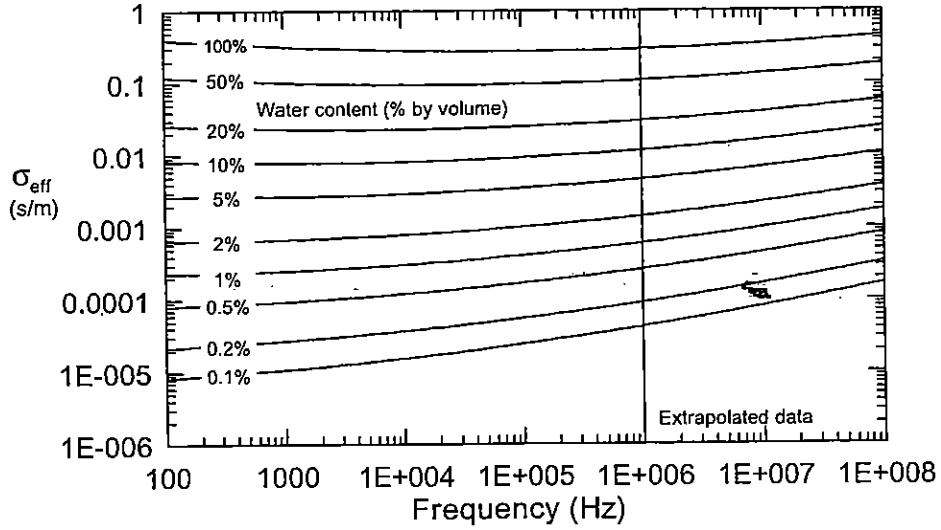

b. Effective conductivity

Figure 1. Plots of the effective relative dielectric constant (a) and the effective conductivity (b) of soil with different water content (by volume), as calculated from Eqs.(1).

2.1.2 *Measurements by Eberle*

Additional studies trying to increase the upper frequency range of the measurements were documented in reports by Eberle [9, 10], in which measurement results from three different sandstone materials were reported [11]. Most notable in these reports was the fact that the measured results were displayed in parametric form, for which a graphical interpolation scheme was provided to be able to determine the earth parameters for an arbitrary frequency and water content. However, for automatic calculation of responses at a large number of frequencies, these data are not particularly convenient to use and they will not be discussed further.

2.1.3 *Jaycor Measurements*

More recent work was reported by Jaycor investigators [12], where they performed measurements on soil obtained near Albuquerque, NM, over a frequency range of 1 kHz to 10 MHz, and then compared the results with those of Scott [8]. Figure 2 presents their measured results for $\varepsilon_{eff}/\varepsilon_o$ and σ_{eff}, and we note a reasonable agreement with the data from Scott in Figure 1.

2.1.4 *Data Presented by King*

While not performing any direct measurements of earth or dielectric properties, King [13] discussed the dielectric and conductive properties of dielectrics and their effects on antennas. He has summarized the behavior of $\varepsilon_{eff}/\varepsilon_o$ and σ_{eff}, as determined by several different investigators, and included them in a summary curve for a clay-loam soil, having a water content of about 10% by weight. These data have been reproduced in Figure 3, where we note that these curves correlate closely with the data provided in the previous figures.

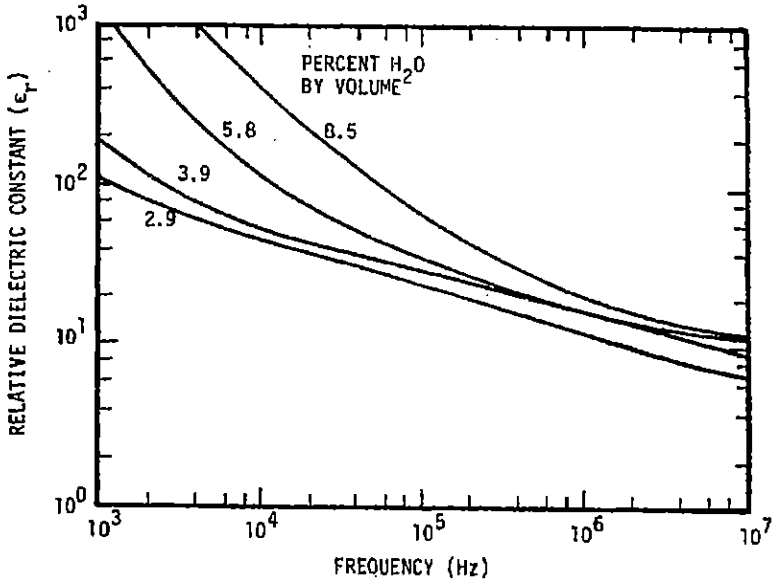

a. Relative effective dielectric constant.

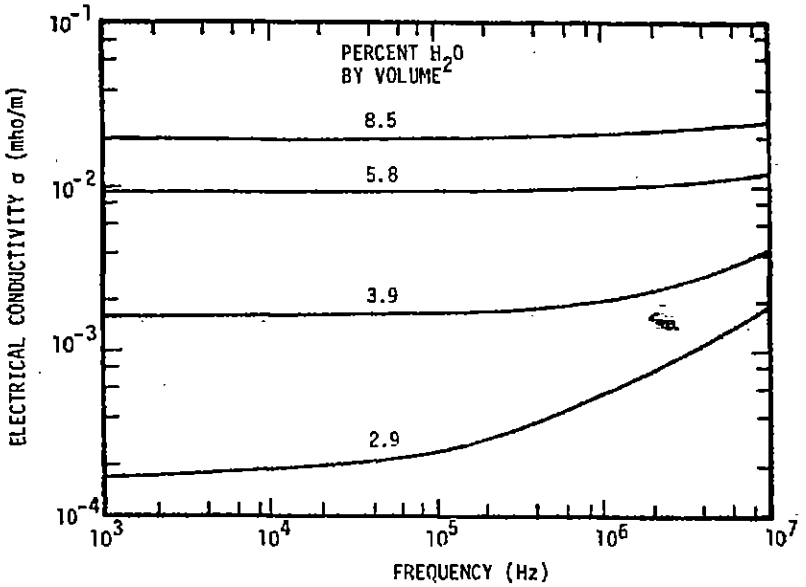

b. Effective conductivity

Figure 2. Plots of the measured effective relative dielectric constant (a) and the effective conductivity (b) of Albuquerque NM sandy soil with different water content (by volume), as reported in [12].

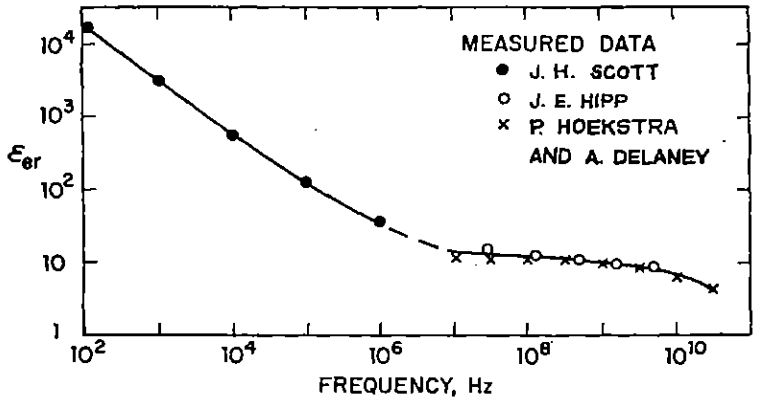

a. Relative effective dielectric constant

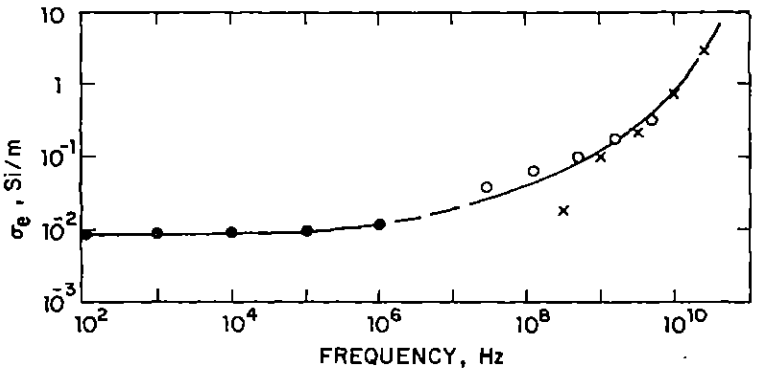

b. Effective conductivity

Figure 3. Plots of a typical effective relative dielectric constant (a) and the effective conductivity (b) of a sandy-clay-loam soil with a 10% (by weight) water content, as reported in [13].

2.2 Enforcement of Causality in Measured Parameters

As noted by Baum [14], the independent measurements of the real-valued parameters ε_{eff} and σ_{eff} over a large bandwidth will contain errors. As such, these parameters can lead to a non-causal transient solution, if they are incorporated in any sort of a frequency domain calculation. This is because the real and imaginary part of the *effective complex permittivity* $\hat{\varepsilon}_{eff}(\omega) = \varepsilon_{eff}(\omega) - j\dfrac{\sigma_{eff}(\omega)}{\omega}$ must obey the Kramer-Kronig relationships given in Eqs.(A25) in Appendix A, and in the presence of measurement error and noise, this relationship may not be

met. Thus, the use of measured data for ε_{eff} and σ_{eff} should take into account the possibility of "correcting" the data to insure causality.

As discussed in the Appendix, one way to do this is to "filter" the measured data with a Hilbert filter to make it causal. The other approach is to fit the data to a functional form known to provide causality. Several investigators, as described below, have used this latter approach.

2.2.1 The Longmire Soil Model

Taking the measured data for $\varepsilon_{eff}/\varepsilon_o$ and σ_{eff} from Scott and fitting it with a series of terms like in Eq.(A29) of Appendix A, Longmire [15] has developed causal representations for the earth parameters. These expressions are given as

$$\frac{\varepsilon_{eff}(\omega)}{\varepsilon_o} = \varepsilon_\infty + 4\pi c \sum_{n=1}^{4} a_n \frac{\beta_n}{(\beta_n^2 + \omega_n^2)} \tag{2}$$

$$\sigma_{eff}(\omega) = \frac{1}{0.3}\left(\sigma_o + \sum_{n=1}^{4} a_n \frac{\omega^2}{(\beta_n^2 + \omega_n^2)}\right) \text{ (s/m)} \tag{3}$$

where the parameters ε_∞ σ_O and a_i are curve-fit parameters given in Table 1 as a function of the water content (by volume) of the soil. The term β_n is a fitting frequency for the terms in the equation and are given by

$$\beta_n = 2\pi 10^{1+n} \text{ (Hz)}, \tag{4}$$

and the parameter c in Eq.(2) is the speed of light, 3.0×10^8 m/s.

Table 1. Fit parameters for ground conductivity and dielectric constant, from Longmire [15].

Water volume (%)	ε_∞	a_1	a_2	a_3	a_4	σ_0
0.3	11.3	1.08×10^{-6}	2.12×10^{-6}	5.10×10^{-6}	2.95×10^{-5}	1.25×10^{-5}
1	16.7	3.86×10^{-6}	5.25×10^{-6}	1.38×10^{-5}	5.15×10^{-5}	7.25×10^{-5}
3	23.3	1.24×10^{-5}	1.49×10^{-5}	3.35×10^{-5}	1.12×10^{-4}	3.75×10^{-4}
10	39.3	5.33×10^{-5}	5.48×10^{-5}	8.88×10^{-5}	2.84×10^{-4}	2.15×10^{-3}
30	74.1	2.07×10^{-4}	1.82×10^{-4}	2.77×10^{-4}	6.27×10^{-4}	1.20×10^{-2}
100	169	1.12×10^{-3}	8.04×10^{-4}	1.01×10^{-3}	1.79×10^{-3}	8.26×10^{-2}

Figure 4 presents a comparison of Scott's data for the relative effective dielectric constant (the solid lines) as a function of frequency, together with the calculated values from Longmire's expression Eq.(2). Similarly, Figure 5 presents a comparison of the effective conductivity. Notice that the agreement between the two is quite good, but that the expressions of Longmire are preferable, as they provide causal results.

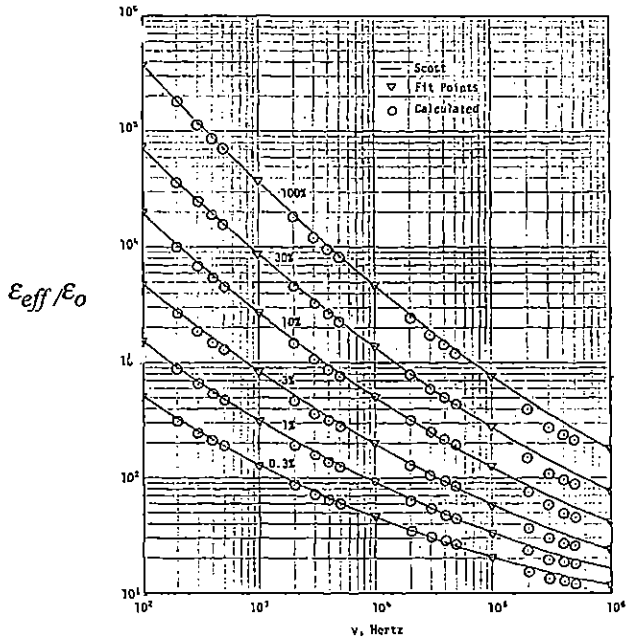

Figure 4. Comparison of the causal curve-fit relative effective dielectric constant of Longmire [15] with the curve-fit data of Scott [8].

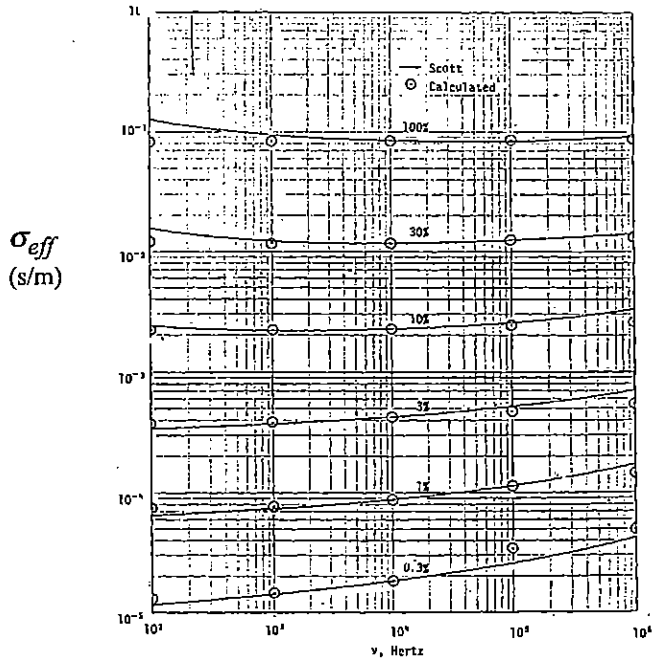

Figure 5. Comparison of the causal curve-fit effective conductivity of Longmire [15] with the curve-fit data of Scott [8].

2.2.2 The Messier Soil Model

In developing an alternative curve-fit solution to the Scott data, Messier [16] discovered that an empirical model for fitting the parameters for ε_{eff} and σ_{eff} given by the expressions

$$\varepsilon_{eff}(\omega) = \varepsilon_{\infty} + \sqrt{\frac{2\sigma_o \varepsilon_{\infty}}{\omega}} \tag{5}$$

and

$$\sigma_{eff}(\omega) = \sigma_o + \sqrt{2\sigma_o \varepsilon_{\infty} \omega} \tag{6}$$

can be rather accurate. Moreover, as discussed by Messier, these expressions can be shown to provide causal results for computed responses, and hence, they obey the Kramer-Kronig relationships. This model for the lossy earth depends only on two parameters: the high frequency dielectric constant ε_{∞}, and on the DC conductivity σ_o (together, of course, with the frequency.) It should be noted that these model parameters could depend on the water content of the soil as given by the data of Scott.

To gain an understanding of the accuracy of the parameters of Eqs.(5) and (6), Figure 6 presents the effective dielectric constant of earth with a 10% water content, using Scott's curve-fit of Eq.(1a), the model from Messier in Eq.(5), and a causally-constructed dielectric constant obtained by using the Kramer-Kronig relationship in Eq.(A26a). For the evaluation of Eq.(5), the following parameters have been assumed:

$$\varepsilon_{\infty} = 7.09\ \varepsilon_0$$

$$\sigma_0 = 8.0 \times 10^{-3}\ \text{(s/m)}.$$

The agreement between these three models is quite good at high frequencies. However, for frequencies less than 1 MHz, the Kramer-Kronig derived dielectric constant is significantly larger than the other two.

Figure 7 presents the effective conductivity, again derived from the expressions of Scott (Eq.(1b)), Messier (Eq.(6)), and from the Kramer-Kronig expression of Eq.(A26b) applied to the dielectric constant of Eq.(1a), which indirectly yields the conductivity through the expression $\mathrm{Im}[\hat{\varepsilon}_{eff}(\omega)] = \frac{\sigma(\omega)}{\omega}$. From these curves, we note that there is good agreement between the causal fit of Messier and the measured data of Scott, but that the Kramer-Kronig fit of the conductivity using the measured dielectric constant deviates significantly from the other two curves.

Thus, it appears that while the Messier fit provides a causal representation for both the dielectric constant and the earth conductivity, the use of the Kramer-Kronig relationships is not as good. Applying either Eq.(A26a) to the conductivity or (A26b) to the effective dielectric constant will provide a causal representation for the other parameter, but there is no guarantee that these results are consistent. Two different sets of causal parameter data result, and if the errors in measurement are large, significant differences in these expressions can be found. Thus, it appears that the use of a causal function curve fit to the data, as opposed to a filtering of the measured data, is the preferred approach for representing the frequency dependence of the earth parameters.

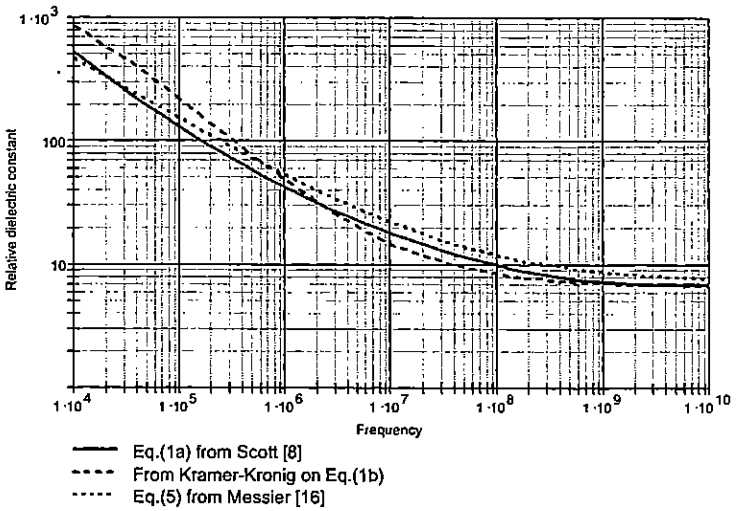

Figure 6. Comparison of the effective dielectric constant $\varepsilon_{eff}(\omega)/\varepsilon_0$ as given by Messier [16] and Scott [8], and calculated from the conductivity of Scott using the Kramer-Kronig relations.

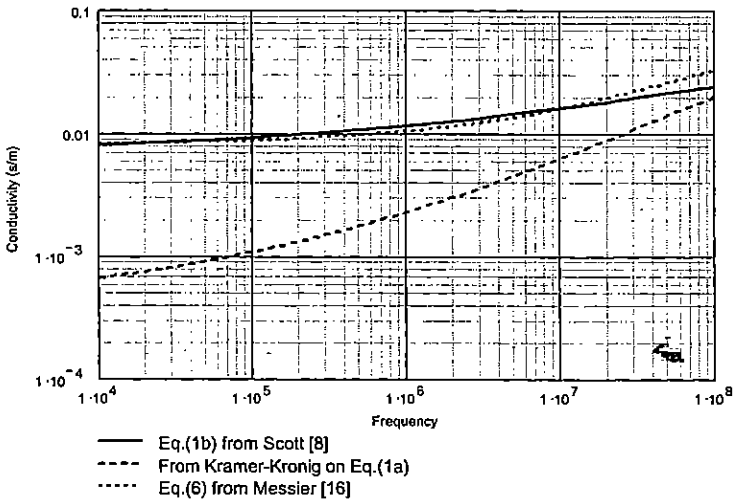

Figure 7. Comparison of the effective conductivity $\sigma_{eff}(\omega)$ as given by Messier [16] and Scott [8], and calculated from the permittivity of Scott using the Kramer-Kronig relations.

2.3 High Frequency Earth Parameter and Models

Recently a measurement program was undertaken to determine the electrical properties of earth material for fast-pulse (sub-nanosecond) applications [17, 18]. This work involved making measurements of the fast-pulse attenuation and dispersion in a coaxial test fixture containing the earth sample, and then fitting the frequency domain dispersion relations obtained by a Fourier transform of the measured transient data to an appropriate model of the dielectric properties.

In this work, the material is represented by the complex effective dielectric constant $\hat{\varepsilon}_{eff}$ defined in Eq.(A22), with either a Debye or a Lorentz model used to represent the behavior of the actual dielectric constant $\varepsilon = \varepsilon' - j\varepsilon''$. The Debye model included the effects of an assumed constant conductivity and took the form

$$\hat{\varepsilon}_{eff} = \varepsilon_o \hat{\varepsilon}_{rel} = \varepsilon_o \left[\varepsilon_\infty + \frac{\varepsilon_s - \varepsilon_\infty}{1 + j\omega\tau} - j\frac{\sigma}{\omega\varepsilon_o} \right], \tag{7a}$$

where the parameters $\varepsilon_\infty, \varepsilon_s, \tau$ and σ are determined by a least squares fit to the measured data. In one case (involving concrete, a slightly more complicated Lorentz model was used. This had the form

$$\hat{\varepsilon}_{eff} = \varepsilon_o \hat{\varepsilon}_{rel} = \varepsilon_o \left[\varepsilon_\infty + (\varepsilon_s - \varepsilon_\infty) \frac{(\alpha^2 + \beta^2)}{(\alpha^2 + \beta^2) + j2\omega\alpha - \omega^2} - j\frac{\sigma}{\omega\varepsilon_o} \right] \tag{7b}$$

where $\varepsilon_\infty, \varepsilon_s, \sigma$, α and β are curve-fit parameters.

Based on the measured responses, ref.[18] provides the curve-fit values for the constitutive parameters for the following earth materials:

- Water
- Dry sand
- Wet sand with a 1.58% (by weight) water content
- Wet sand with a 3.32% (by weight) water content
- Concrete

These parameters required for these materials are summarized in Table 2.

Table 2. Curve-fit parameters for various materials, based on measurements from Farr[18].

Material	ε_∞	ε_S	τ (ps)	σ (s/m)	α (ns-1)	β (ns-1)
WATER[1]	23.4606	81.8358	9.4	0.0	----	----
DRY SAND[1]	2.4725	2.5160	17.3	1.5526×10^{-3}		----
MOIST 1.58% SAND[1]	2.1413	2.6825	5.5	1.3828×10^{-3}	----	----
MOIST 3.23% SAND[1]	2.6181	3.1778	11.3	2.857×10^{-3}	----	----
CONCRETE[2]	1.995×10^{-5}	3.4406	---	7.6335×10^{-3}	9.8509	318.446

Notes: 1: Debye model
2: Lorentz model

Plots of the frequency domain behavior of the real and imaginary parts of the complex effective dielectric constant $\hat{\varepsilon}_{eff}$ for the five earth materials are presented in Figure 8. Because the measurements were performed using fast-rising pulses, there is limited low frequency information available in the response spectrum; consequently, these material responses end at a low frequency of 1 MHz. Furthermore, the increase in the dielectric constant at very low frequencies is not evident with this model.

To permit a comparison of these measurements with the data discussed earlier, it is useful to translate the real and imaginary parts of $\hat{\varepsilon}_{eff}$ into the real valued effective dielectric constant and conductivity ε_{eff} and σ_{eff} defined in Eq.(A20). This relationship is

$$\varepsilon_{eff} = \mathrm{Re}\left[\hat{\varepsilon}_{eff}\right] \; and \; \sigma_{eff} = -\omega\varepsilon_o \, \mathrm{Im}\left[\hat{\varepsilon}_{eff}\right]. \tag{8}$$

Figure 9 plots the quantities $\varepsilon_{eff}/\varepsilon_O$ and σ_{eff} for these materials from the data given in Figure 8.

Comparing the results from this model with those of Scott [8] is not easy, due to the different frequency ranges of the data. However, both sets of data include the common frequency of 1 MHz, and a comparison at this frequency is possible. In comparing Figure 9 with Figure 1, we note that there is about a factor of 10 difference in the dielectric constants for a soil sample with a water content of about 3%. However, a comparison of the electrical conductivities in part *b* of the figures shows a much better correlation.

For HEMP applications, the low frequency behavior of the constitutive parameters appears to be more important, because the frequency spectrum of the excitation falls off rapidly at the higher frequencies above about 50 MHz. Thus, in the sensitivity study that follows, we will adapt the low frequency relationships in Eq.(1) from Scott, with an extrapolation process for determining the parameters for frequencies greater than 1 MHz.

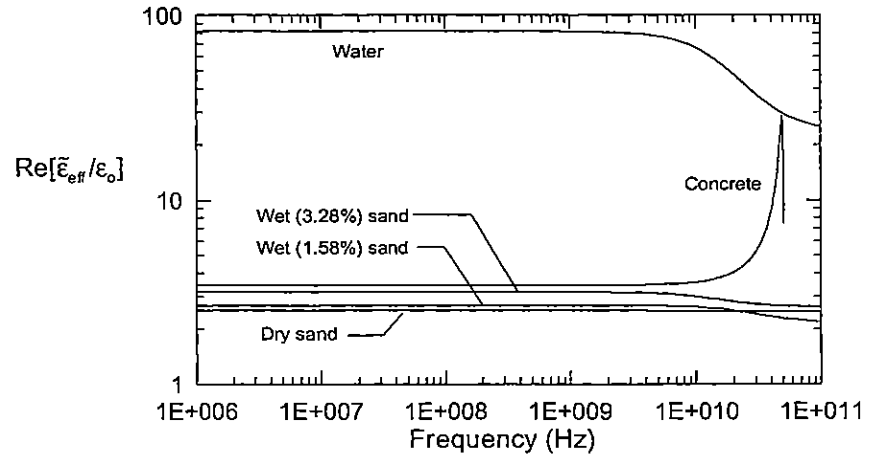

a. Real part

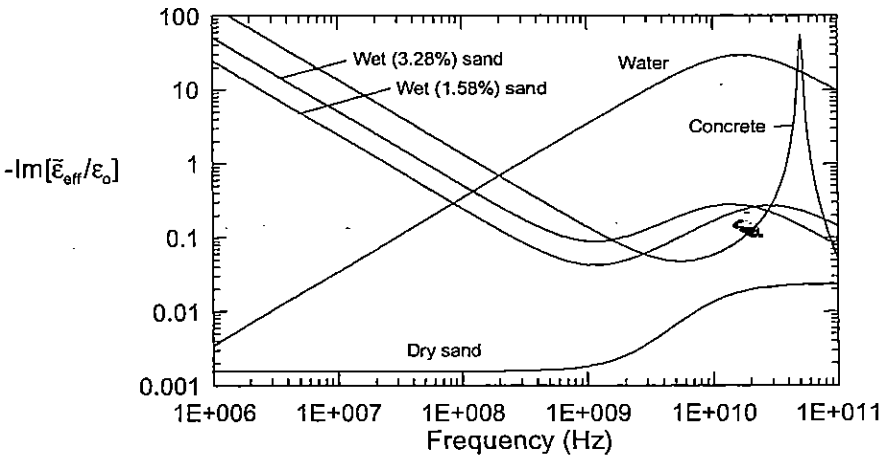

b. Imaginary part

Figure 8. Plots of the real part (a) and imaginary part (b) of the complex effective dielectric constant $\tilde{\varepsilon}_{eff}$ for different earth materials, as reported in ref.[18].

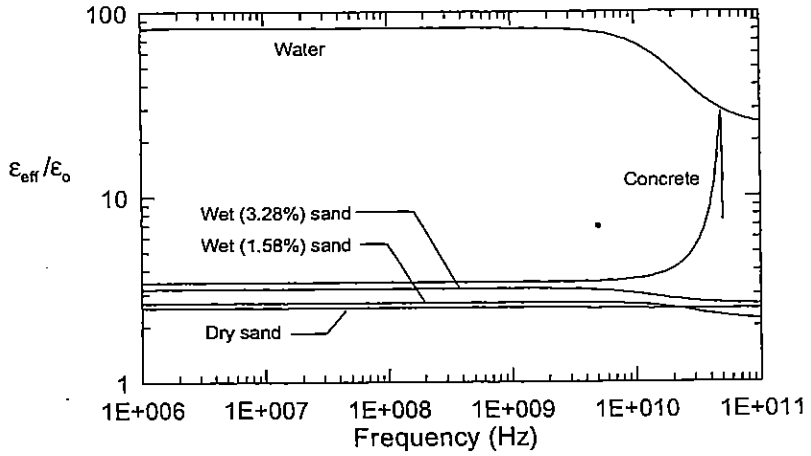

a. Relative dielectric constant $\varepsilon_{eff}/\varepsilon_O$

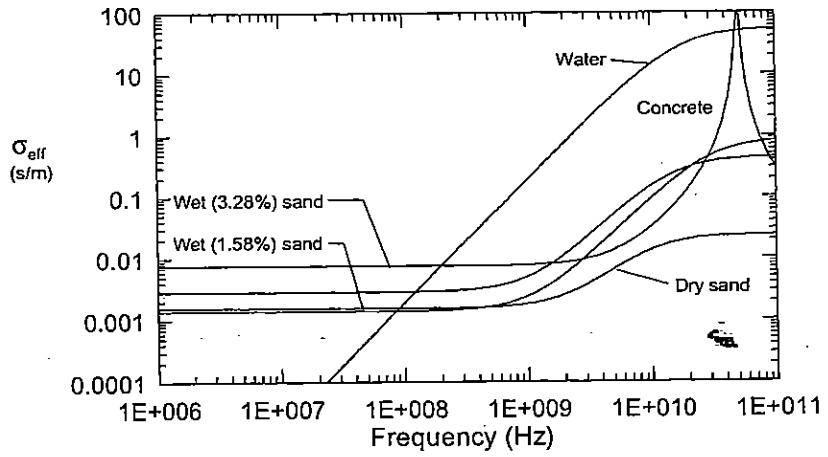

b. Effective conductivity

Figure 9. Plots of the real-valued effective relative dielectric constant (a) and effective conductivity of the material of Figure 8.

3. Effects of Earth Parameters on EM Field Solutions

It is clear that the different earth models will provide different solutions for wave propagation in the earth. In this section, we examine the effects of these models on the frequency dependent propagation constant and wave impedance in the soil, as well as the effects on transient solutions.

3.1 Propagation Constant and Impedance in the Soil

As an example of the effects of frequency variations in the constitutive parameters ε and σ, it is instructive to examine the behavior of the plane wave propagation constant γ and the characteristic wave impedance Z_c. These quantities are given by

$$\begin{aligned}\gamma(\omega) &= \sqrt{(j\omega\mu_o)(j\omega\varepsilon_{eff}(\omega)+\sigma_{eff}(\omega))} \\ &= j\omega\sqrt{\mu_o\varepsilon_o}\left[\sqrt{\kappa(\omega)-j\frac{\sigma_{eff}(\omega)}{\varepsilon_o\omega}}\right] \\ &= jk_o\sqrt{\kappa(\omega)-j\frac{\sigma_{eff}(\omega)}{\varepsilon_o\omega}}\end{aligned} \tag{9}$$

and

$$\begin{aligned}Z_c(\omega) &= \sqrt{(j\omega\mu_o)/(j\omega\varepsilon(\omega)+\sigma(\omega))} \\ &= \frac{Z_o}{\sqrt{\kappa(\omega)-j\frac{\sigma(\omega)}{\varepsilon_o\omega}}}\end{aligned} \tag{10}$$

where $k_o = \omega\sqrt{\mu_o\varepsilon_o}$ is the free space propagation constant, $Z_o = \sqrt{\mu_o/\varepsilon_o}$ is the wave impedance of free space, and κ is the *relative effective dielectric constant* defined through the expression $\varepsilon_{eff}(\omega) \equiv \kappa(\omega)\varepsilon_o$.

Figure 10 plots the real and imaginary parts of the propagation constant γ in Eq.(9) for the soil having water contents ranging from 0.1% to 100% (by volume), as calculated for the constitutive parameters of Scott using Eq.(1). A commonly used set of frequency independent earth parameters is $\kappa = 10$ and $\sigma = 0.01$ s/m. In examining Figure 1, we note that the value of ground conductivity of 0.01 s/m corresponds roughly to water content of 10 % in the soil. The correspondence with the relative dielectric constant in Figure 1a, however, is not particularly good.

The real part of the propagation constant, shown in Figure 10a relates to the attenuation of a plane wave traveling through the earth. We note that there is a rather good correlation between this attenuation constant for a constant parameter earth model and the 10% water

model for low frequencies (up to about 10 MHz). However, as the frequency increases, the displacement current in the soil becomes more important, and the difference in the effective dielectric constant becomes apparent. Evidently, the frequency dependent soil model provides larger attenuation for the waves at high frequencies than does the fixed parameter mode.

The imaginary part of γ corresponds to the propagation of the waves in the medium. As seen in Figure 10b, there is a generally good agreement with the results from the constant parameter model and the 10% water model.

Figure 11 presents a similar comparison of the real and imaginary parts of the characteristic wave impedance given by Eq.(10). We note that there is poor agreement between the fixed parameter model (for $\kappa = 10$ and $\sigma = 0.01$ s/m) and the 10% water content model for $f < 10$ MHz, presumably due to the very large relative dielectric constant in the soil at these low frequencies.

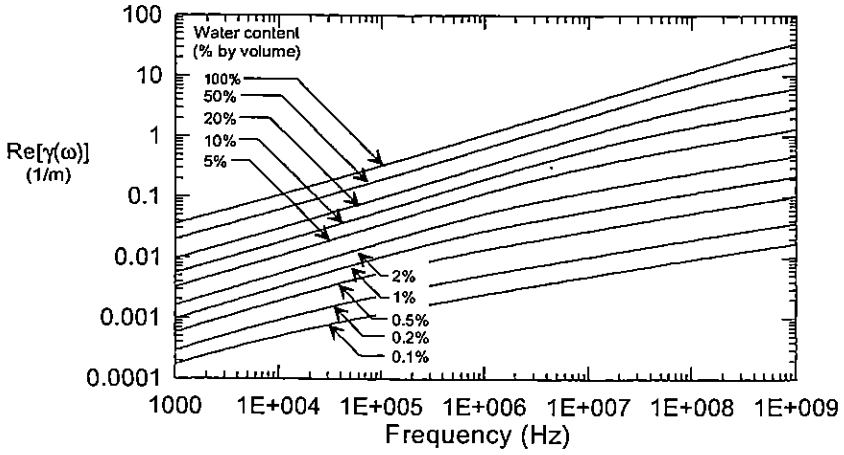

a. Real part

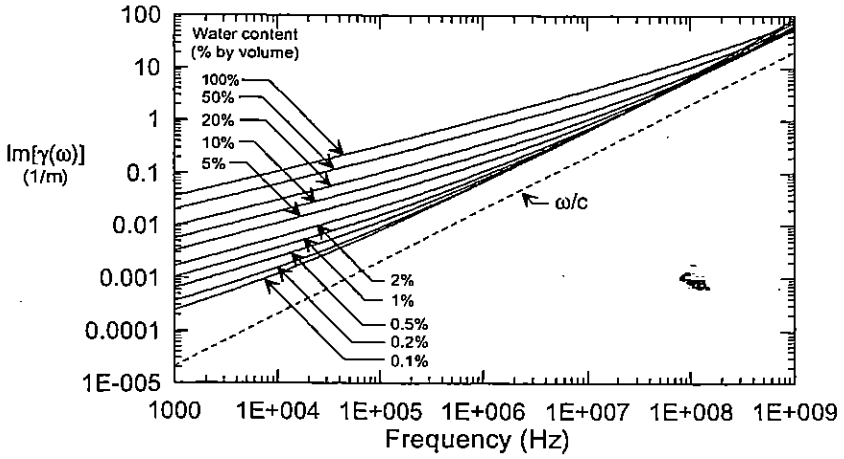

b. Imaginary part

Figure 10. Plot of the real part (a) and imaginary part (b) of the propagation constant in the soil for different water contents, as calculated for the constitutive parameters of Scott from Eq.(1).

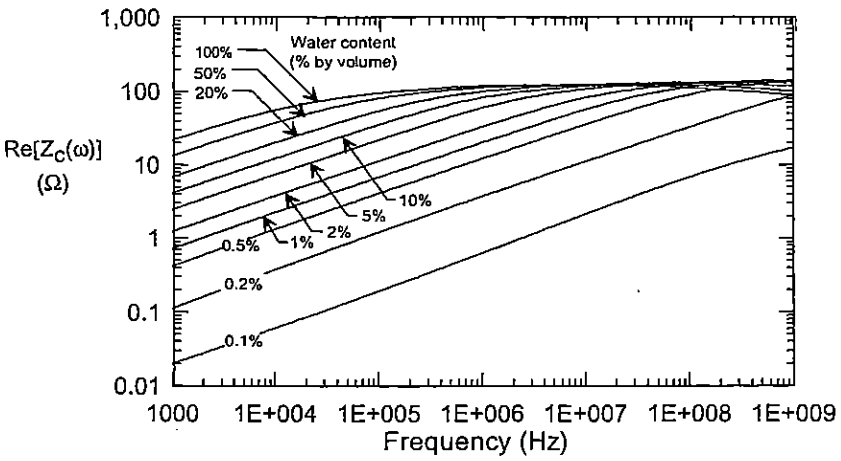

a. Real part

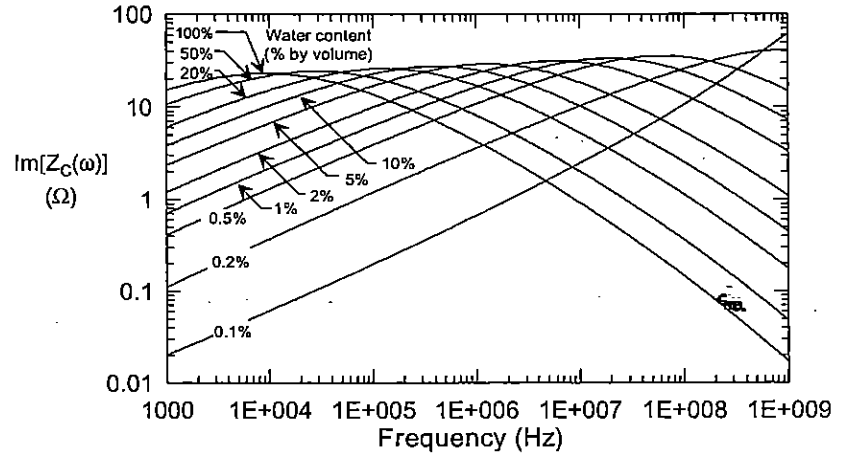

b. Imaginary part

Figure 11. Plot of the real part (a) and imaginary part (b) of the wave impedance in the soil for different water contents, as calculated for the constitutive parameters of Scott from Eq.(1).

Using the Messier model for the earth parameters, the propagation constant in Eq.(9) can be written in the following form:

$$\gamma(\omega) = j\omega\sqrt{\mu_o\varepsilon_\infty} + \sqrt{j\omega\mu_o\sigma_o}$$
$$= \sqrt{\frac{\mu_o\sigma_o\omega}{2}} + j\left[\omega\sqrt{\mu_o\varepsilon_\infty} + \sqrt{\frac{\mu_o\sigma_o\omega}{2}}\right], \qquad (11)$$

which is seen to provide a simple time shift component given by the term $j\omega\sqrt{\mu_o\varepsilon_\infty}$, and a diffusive component given by the $\sqrt{j\omega\mu_o\sigma_o}$ term. This provides for a relatively simple view of pulse propagation within the earth.

To illustrate the behavior of the propagation constant as a function of frequency for these earth models, Figure 12 plots the real and imaginary parts of the propagation constant in the soil having *constant* parameters of ε_r = 7.09 and σ .= 8.0 × 10^{-3} (s/m), the frequency dependent Messier model with parameters ε_∞ = 7.09 and σ_0.= 8.0 × 10^{-3} (s/m), and the Scott model from Eq.(1) with a 10% water content. Also shown in part (b) is the free-space propagation constant ω/c, which is the straight line.

Similar data are shown for the wave impedance in Figure 13

From these plots we note that there is a rather good agreement between the Scott data and the Messier model over a wide frequency range. However, for frequencies above about 10 MHz, the constant parameter model results deviate from the others. As this frequency range is still of importance in NEMP problems, we will expect that transient responses using these different models will exhibit some differences. This will be examined in the next section.

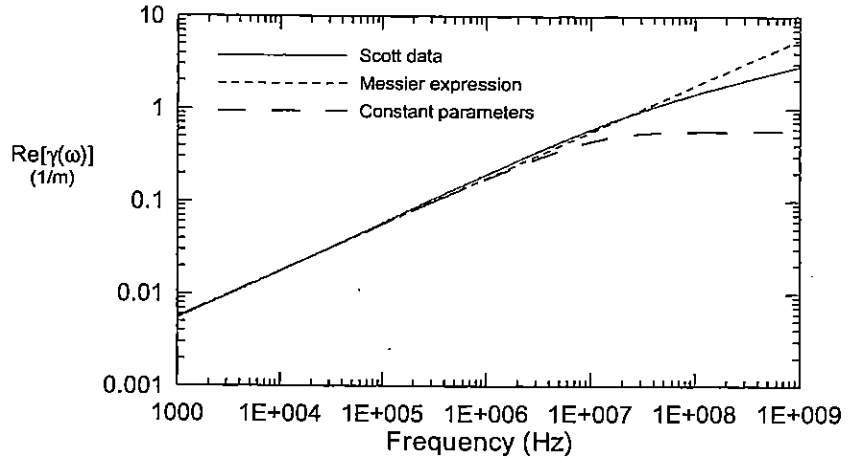

a. Real part

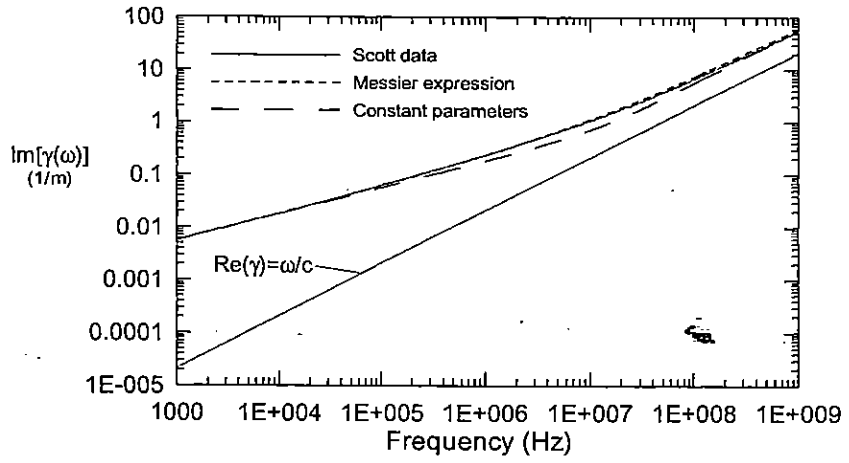

b. Imaginary part

Figure 12. Plot of the real part (a) and imaginary part (b) of the propagation constant in the soil having constant parameters of $\varepsilon_r = 7.09$ and $\sigma = 8.0 \times 10^{-3}$ (s/m) (the dashed line), the frequency dependent Messier model with parameters $\varepsilon_\infty = 7.09$ and $\sigma_0 = 8.0 \times 10^{-3}$ (s/m) (the thin solid line), and the Scott model from Eq.(1) with a 10% water content (dotted line).

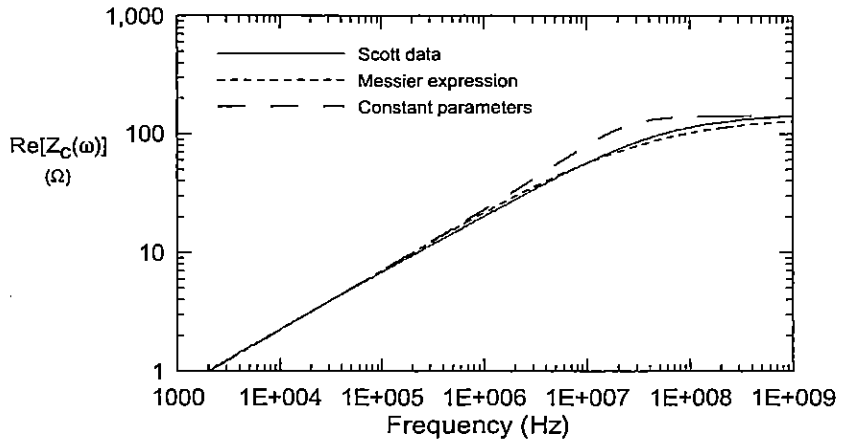

a. Real part

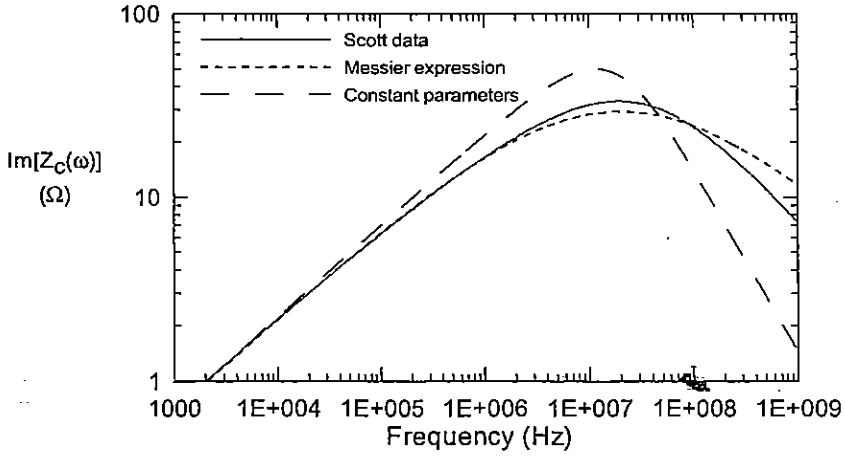

b. Imaginary part

Figure 13. Plot of the real part (a) and imaginary part (b) of the wave impedance in the soil having constant parameters of $\varepsilon_r = 7.09$ and $\sigma = 8.0 \times 10^{-3}$ (s/m) (the dashed line), the frequency dependent Messier model with parameters $\varepsilon_\infty = 7.09$ and $\sigma_0 = 8.0 \times 10^{-3}$ (s/m) (the thin solid line), and the Scott model from Eq.(1) with a 10% water content (dotted line).

3.2 Comparison of Reflected and Transmitted Transient Fields

While it is clear from the results of the previous section that there is a difference in the propagation constant and the wave impedance depending of the models used for the parameters ε_r and σ, it is instructive to consider the observed effects on a transient EM field response above or in the earth. In this example, we again assume a constant parameter earth, defined by the parameters of $\varepsilon_r = 7.09$ and $\sigma = 8.0 \times 10^{-3}$ (s/m), the frequency dependent Messier model with parameters $\varepsilon_\infty = 7.09$ and $\sigma_0 = 8.0 \times 10^{-3}$ (s/m), and the Scott model, assuming a 10% water content.

To illustrate the geometry assumed for this example, Figure 14 shows an incident plane wave having either a horizontal or vertical polarization of the E-field vector, propagating downward with a $-z$ component of the propagation vector. It is incident on the lossy earth with angles of incidence ψ and ϕ, and upon striking the ground, it produces both a reflected field with angles $\psi_r = \psi$ and $\phi_r = \phi + 180°$, and a transmitted field at angles ψ_t and $\phi_t = \phi + 180°$.

General expressions for the E and H-field components above and below the ground as a function of the earth parameters and angles of incidence are provided in ref.[19]. For the example considered here, we chose the simple case of a vertically polarized, normally incident field ($\psi = 90°$) with $\phi = 0°$. In this manner, the component of the E-field that is of interest is E_x, and this will be examined both above and below the earth surface.

For this example, three different transient waveforms are considered, each of which is expressed in terms of a double exponential expression of the form

$$E(t) = E_o \Gamma \left(e^{-\alpha t} - e^{-\beta t} \right). \qquad (12)$$

In this expression, α and β are time constants of the waveform and Γ is a normalizing constant, which is chosen so that the true peak value of the waveform is given by E_o.

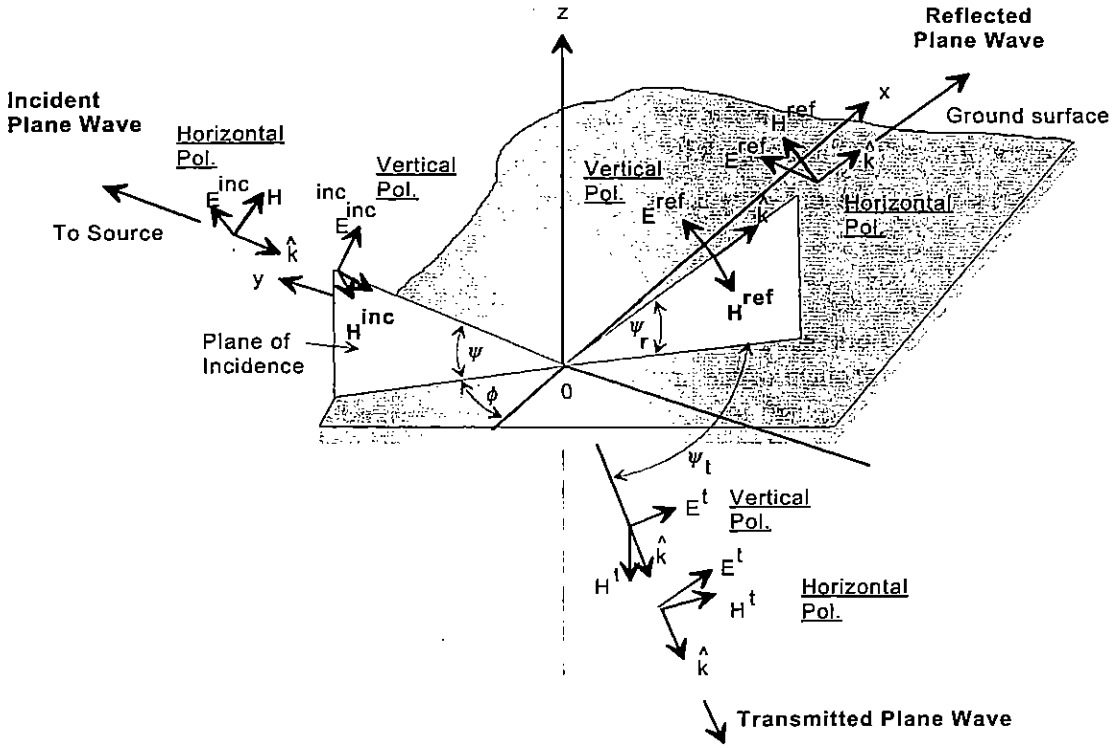

Figure 14. Illustration of a plane wave incident on a lossy earth.

Table 3 presents the parameters α and β used to define the waveforms. Waveform #1 is a fast pulse, having a time to peak of 2.93 ns, and a total waveform time of 1 μs (i.e., the time window over which the transient response is calculated). This pulse would be roughly representative of the behavior of a NEMP field.

Waveforms #2 and #3 are progressively slower, with α and β decreasing by one order of magnitude for each waveform. Figure 15 presents a plot of these waveforms, each normalized by the peak value E_o.

Table 3. Waveform parameters

Waveform	α (1/μs)	β (1/μs)	T_{max}(μs)	T_{peak}(ns)
1	75	1000	1	2.93
2	7.5	100	10	29.3
3	0.75	10	100	293

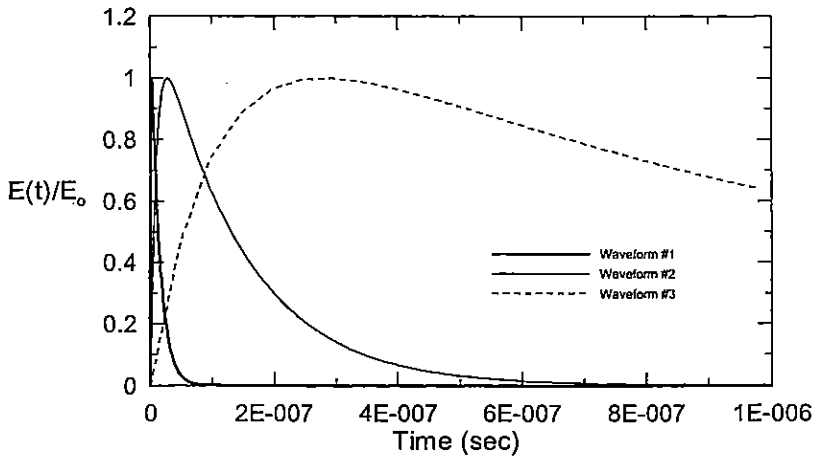

Figure 15. Illustration of the fast, intermediate and slow waveforms.

3.2.1 Reflected Fields

For each of the incident field waveforms of Figure 15, its spectrum is evaluated using a Fourier transform. These spectra are then applied to the expressions for the total E-fields above and below the earth, and the resulting transient response reconstructed using an inverse transform. Considering first the behavior of the above-ground fields at a height $z = 5$ m, Figure 16a presents the transient E_x field for the fast waveform #1. The thick trace represents the result for the frequency-independent earth model, while the dotted line is for frequency dependent Messier model for the earth parameters. The dashed line represents the Scott model response, while the solid thin trace represents the incident field.

In these responses, it is clear that for early times (before the reflected field from the earth has a chance to arrive back at the observer), there should be no difference in between the three curves. This fact is evident in the plot. After the reflection from the earth arrives (at $t = 3.333 \times 10^{-8}$ sec), however, we note that the reflected field *cancels* with part of the incident field and the E_x field decreases in value. In examining the responses of the Scott and Messier earth models in this time regime, we note that there is only a slight difference between the responses. However, the constant earth model shows a roughly 15% difference in the second peak value. This difference is rather small, however, and it probably would be unimportant in most coupling problems.

The frequency domain spectral magnitude for the E_x field for these earth models, together with that of the incident field are presented in Figure 16b.

Similar plots for waveforms #2 and #3 are presented in Figure 17 and Figure 18. From these examples, it is apparent that the above-ground E-field response is not very dependent on the type of earth model used -- as long as the constant earth conductivity and dielectric constant are representative of the actual earth values.

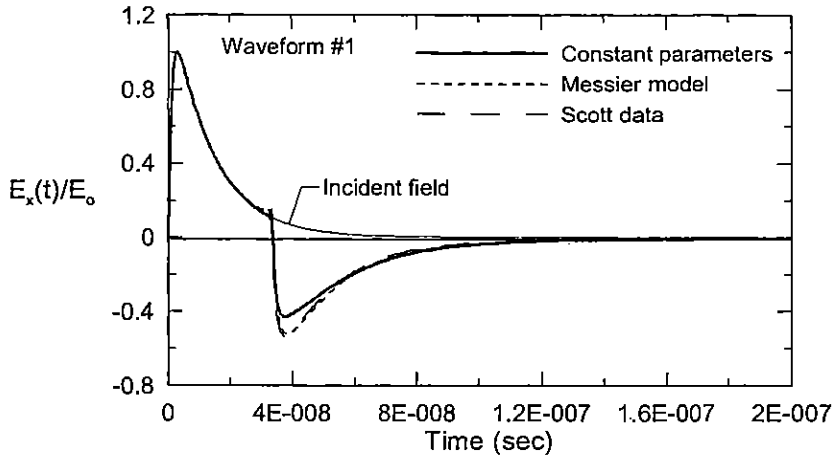

a. Time domain response

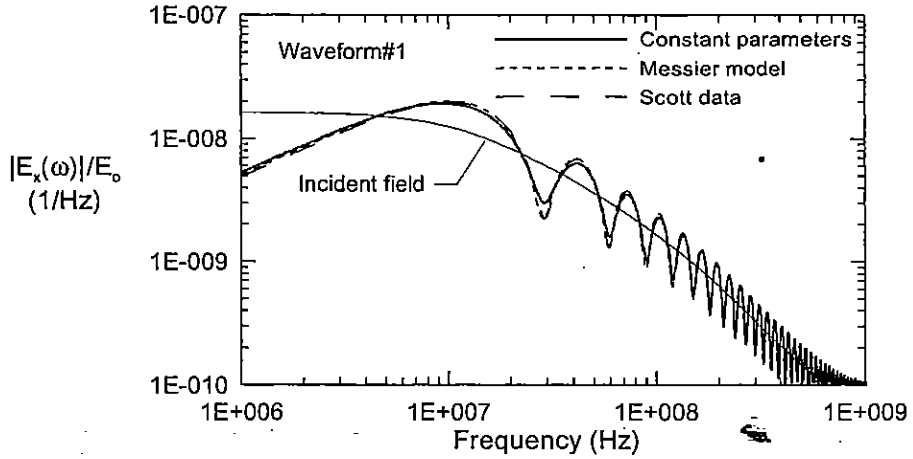

b. Frequency domain spectrum

Figure 16. Plot of the total E_x-field component for waveform #1 at h = 5 m above the soil having constant parameters of ε_r = 7.09 and σ .= 8.0 $\times 10^{-3}$ (s/m) (thick solid line), the frequency dependent Messier model with parameters ε_∞ = 7.09 and σ_0.= 8.0 $\times 10^{-3}$ (s/m) (dotted line), and the Scott model from Eq.(1) with a 10% water content (dashed line).

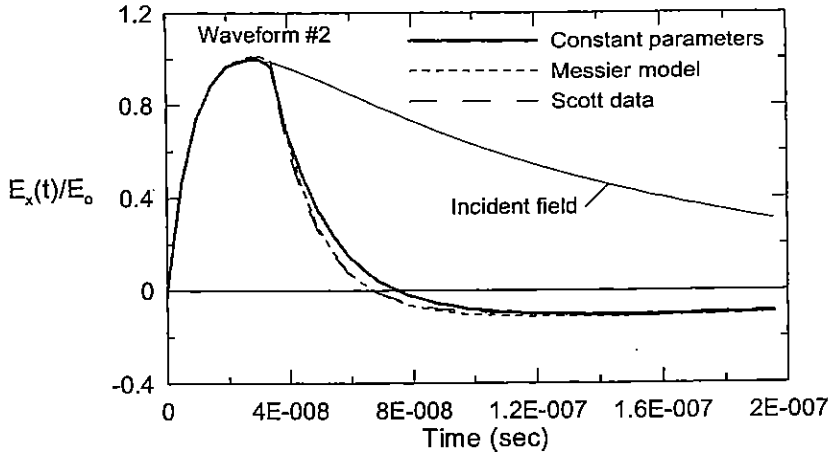

a. Time domain response

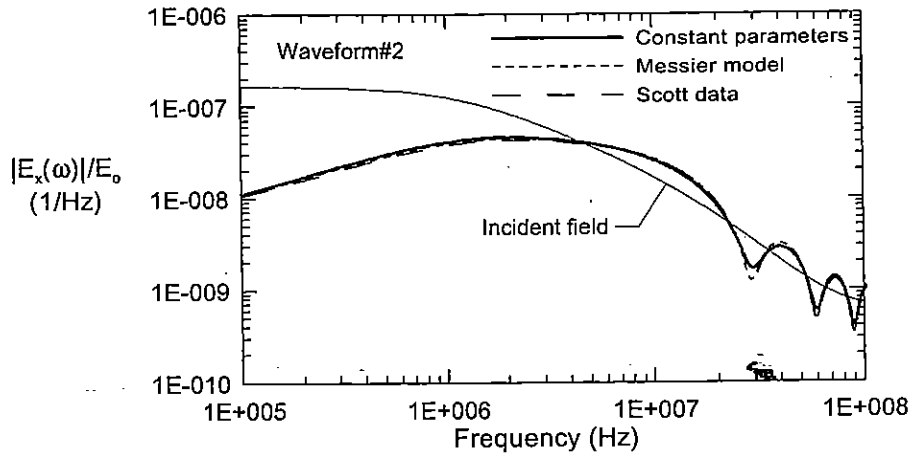

b. Frequency domain spectrum

Figure 17. Plot of the total E_x-field component for waveform #2 at h = 5 m above the soil having constant parameters of ε_r = 7.09 and σ .= 8.0 $\times 10^{-3}$ (s/m) (thick solid line), the frequency dependent Messier model with parameters ε_∞ = 7.09 and σ_0.= 8.0 $\times 10^{-3}$ (s/m) (dotted line), and the Scott model from Eq.(1) with a 10% water content (dashed line).

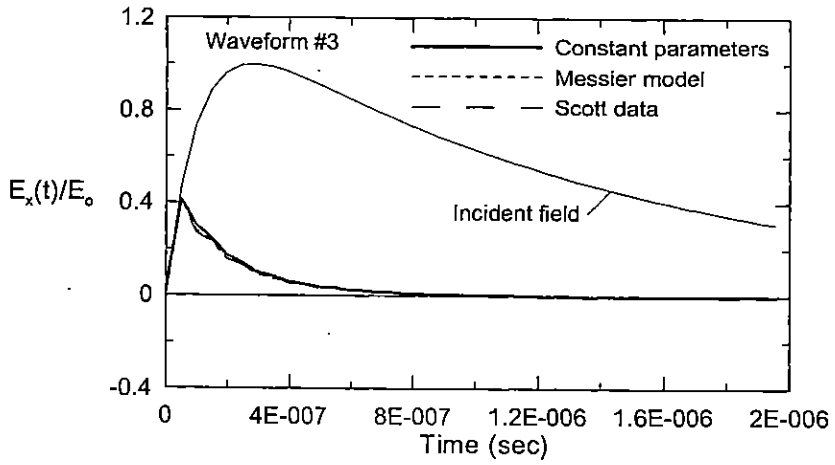

a. Time domain response

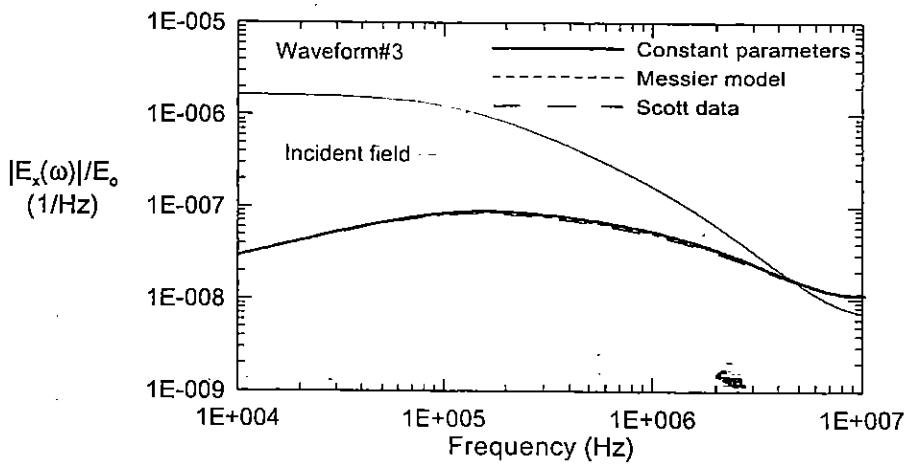

b. Frequency domain spectrum

Figure 18. Plot of the total E_x-field component for waveform #3 at h = 5 m above the soil having constant parameters of ε_r = 7.09 and σ .= 8.0 $\times 10^{-3}$ (s/m) (thick solid line), the frequency dependent Messier model with parameters ε_∞ = 7.09 and σ_0.= 8.0 $\times 10^{-3}$ (s/m) (dotted line), and the Scott model from Eq.(1) with a 10% water content (dashed line).

3.2.2 Fields in the Earth

Similar calculations for the three waveforms of Figure 15 have been performed at a field observation point located within the earth at a distance $z = -5$ m. These responses are presented in Figure 19—Figure 22.

As one might expect, the effect of the earth model is more noticeable in this case, due to the fact that the observation location is directly imbedded in the earth. Notice also that the differences between the constant earth and Messier model are more pronounced for waveform #1 (the fast waveform), due to the fact that this waveform has more high frequency components that do the others, and the models differ significantly at high frequencies.

A careful examination of the early time responses for waveform #1 in Figure 20 shows that both the constant earth model and the Messier model provide causal responses. However, in the Scott model there is a very slight initial negative-going waveform component, which is a result of the non-causal data.

It is clear that there is a constant earth model does not provide results that compare well with those of the presumably more accurate frequency dependent models of Messier and Scott. As a consequence, it is interesting to examine the variations in the constant parameter earth model as the conductivity is varied from 0.008 to 0.02 s/m, with the dielectric constant remaining fixed at $\varepsilon_r = 7.09$. Figure 23 plots these transient responses for the three different excitation waveforms. From these sets of curves, it is clear that a simple shift of the constant conductivity is not sufficient to provide a good agreement of the constant parameter model. Evidently, a frequency dependent earth model is needed for accurate waveform calculations at observation locations within the earth.

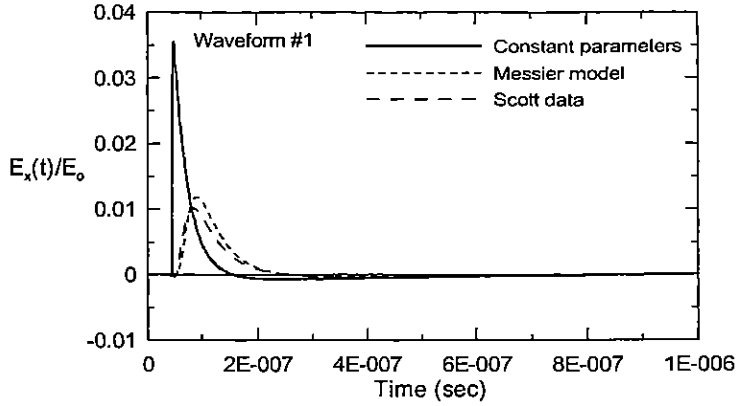

a. Transient responses

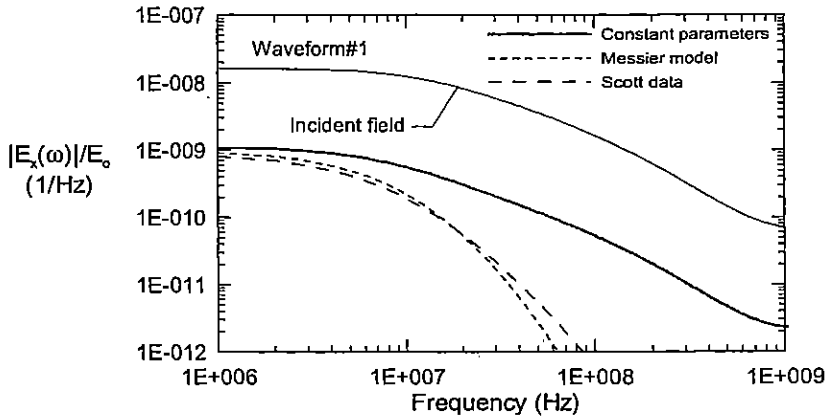

b. Spectral magnitudes

Figure 19. Plot of the total E_x-field component for waveform #1 at h = –5 m within the earth having constant parameters of ε_r = 7.09 and σ .= 8.0 $\times 10^{-3}$ (s/m) (thick solid line), the frequency dependent Messier model with parameters ε_∞ = 7.09 and σ_0.= 8.0 $\times 10^{-3}$ (s/m) (dotted line), and the Scott model from Eq.(1) with a 10% water content (dashed line).

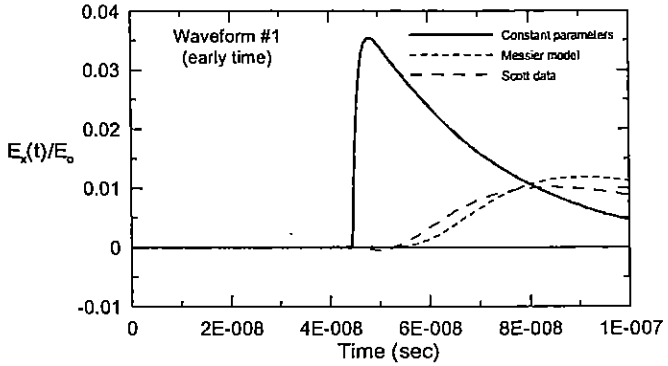

Figure 20. The early time behavior of the waveforms of Figure 19.

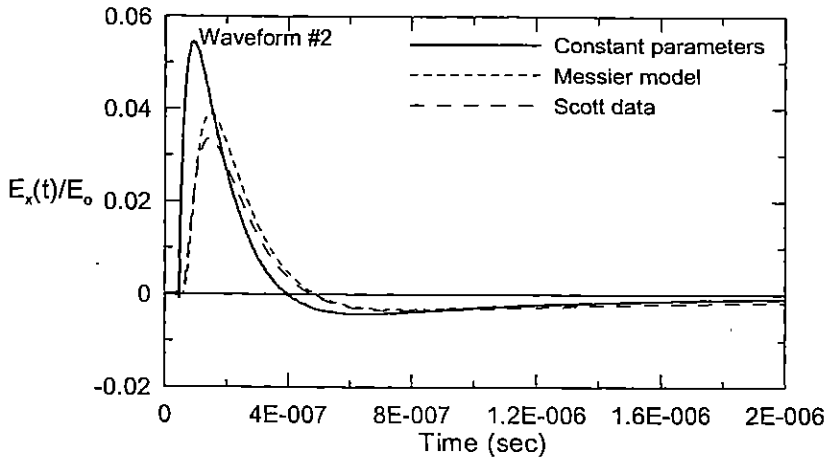

a. Transient responses

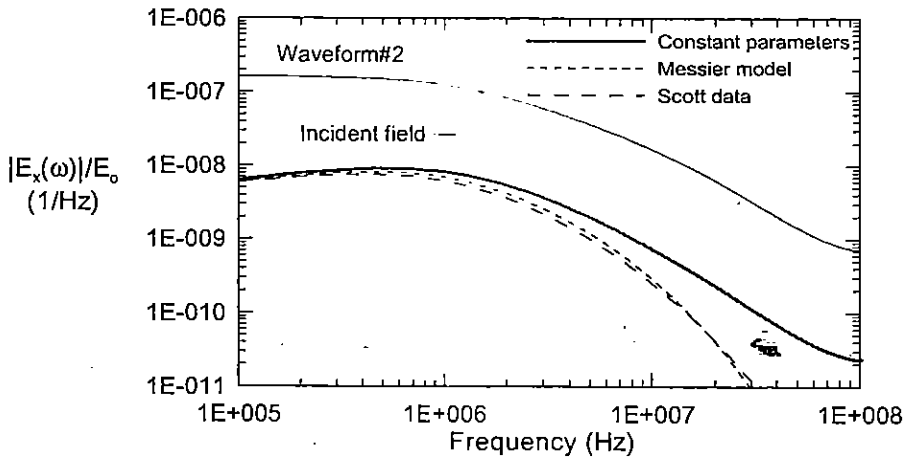

b. Spectral magnitudes

Figure 21. Plot of the total E_x-field component for waveform #2 at $h = -5$ m within the earth having constant parameters of $\varepsilon_r = 7.09$ and $\sigma = 8.0 \times 10^{-3}$ (s/m) (thick solid line), the frequency dependent Messier model with parameters $\varepsilon_\infty = 7.09$ and $\sigma_0 = 8.0 \times 10^{-3}$ (s/m) (dotted line), and the Scott model from Eq.(1) with a 10% water content (dashed line).

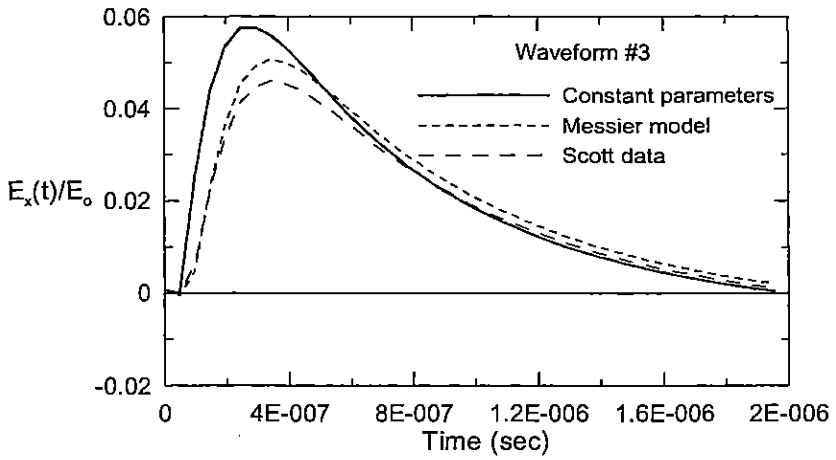

a. Transient responses

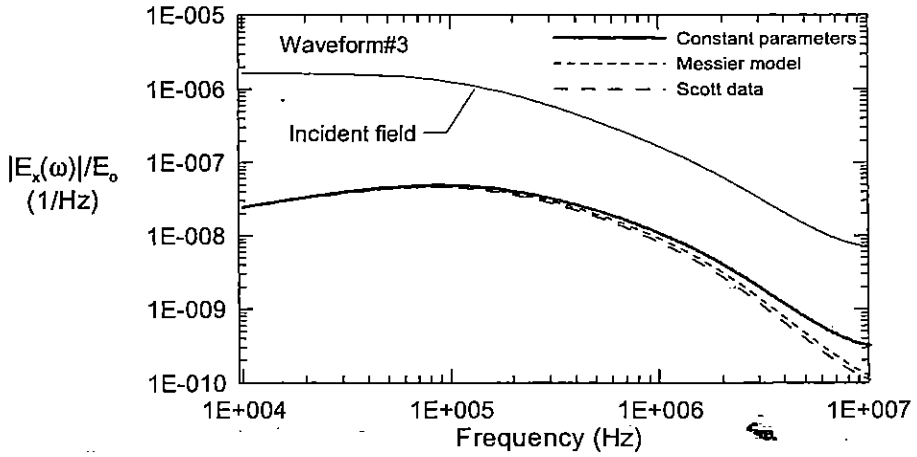

b. Spectral magnitudes

Figure 22. Plot of the total E_x-field component for waveform #3 at h = –5 m within the earth having constant parameters of ε_r = 7.09 and σ .= 8.0 $\times 10^{-3}$ (s/m) (thick solid line), the frequency dependent Messier model with parameters ε_∞ = 7.09 and σ_0.= 8.0 $\times 10^{-3}$ (s/m) (dotted line), and the Scott model from Eq.(1) with a 10% water content (dashed line).

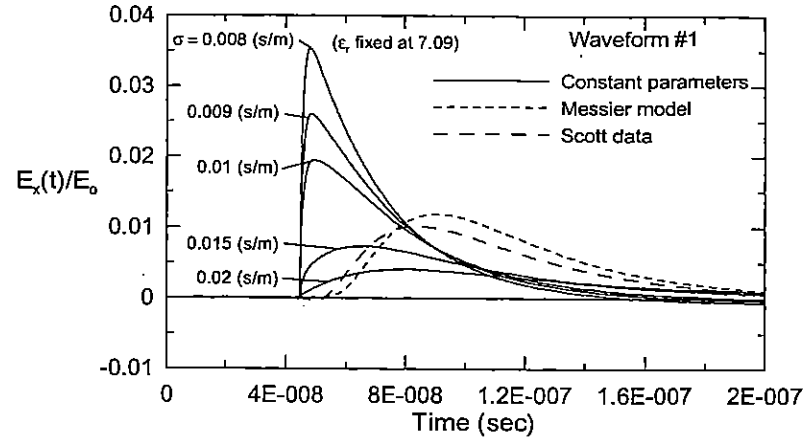

a. Waveform #1

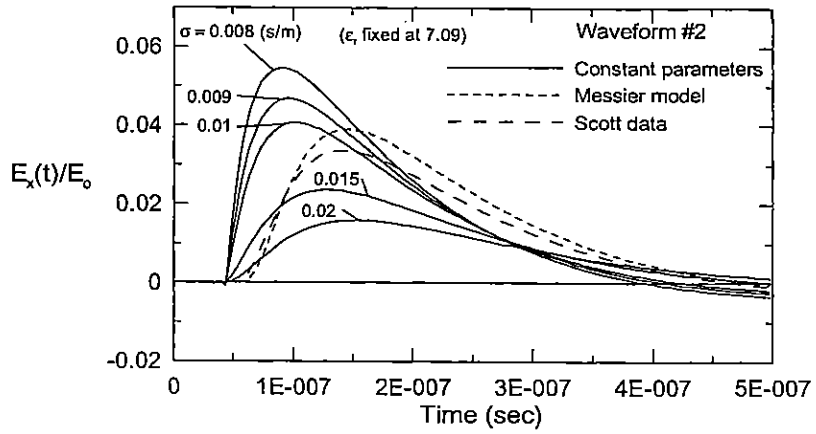

b. Waveform #2

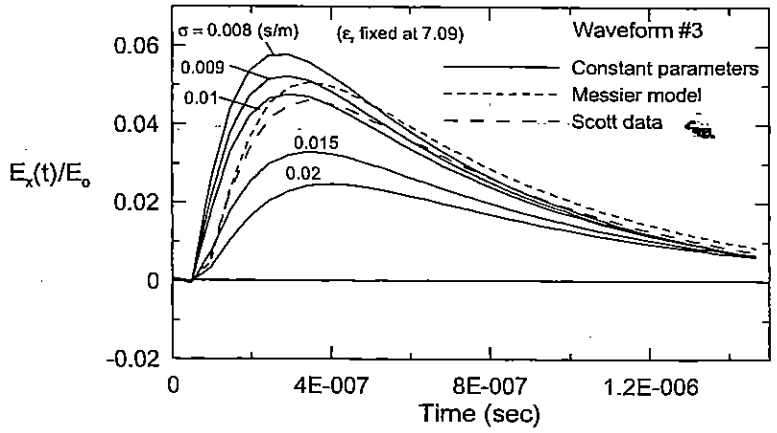

c. Waveform #3

Figure 23. Plots of the transient responses for the three excitation waveforms with a variation of the conductivity of the constant earth model, maintaining the dielectric constant fixed.

3.3 Effects of the Ground Model on Overhead Line Coupling

A further calculation of interest is to examine the behavior of the ground model on the responses of an aboveground transmission line. This is important, since the ground parameters affect both the excitation fields of the line through the reflection coefficient, as well as the propagation constant of waves on the line due to the earth impedance of the line [19].

Figure 24 illustrates the geometry of an aboveground line of length L, height h and wire radius a being illuminated by an incident transient plane wave. The analysis of this line has been discussed in [19] and the computer code RISER has been provided for conducting this analysis. Of particular interest is the induced current I_R flowing at the top of the vertical riser at the $x = L$ end of the line.

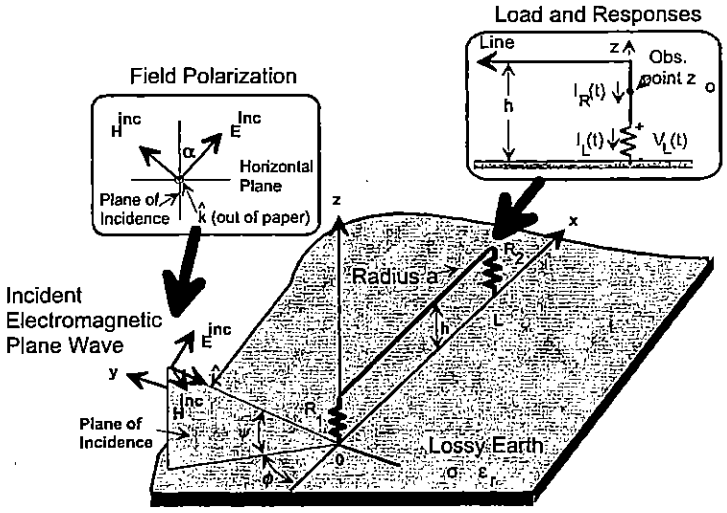

Figure 24. Illustration of an above-ground transmission line as provided by the RISER code.

For this study, the three waveforms in Table 3 have been applied to the line, which had the following parameters

Line length: $L = 5$m
Line height: $h = 0.8$ m
Wire radius: $a = 0.15$ cm
Load resistances: $R_1 = R_2 = 20\ \Omega$
Vertical angle of incidence: $\psi = 45°$
Azimuthal angle of incidence: $\phi = 0°$
E-field polarization angle: $\alpha = 0°$
Earth #1: Constant parameters $\varepsilon_r = 7.09$ and $\sigma = 8.0 \times 10^{-3}$ (s/m)
Earth #2: Messier model with parameters $\varepsilon_\infty = 7.09$ and $\sigma_0 = 8.0 \times 10^{-3}$ (s/m)

The RISER code was modified to permit the use of the Messier earth model, and calculations of the riser current were made. For waveform #1, Figure 25 presents the late time calculated transient riser currents for both the constant earth and the Messier models, extending out to 1 μs. The most noticeable differences between these waveforms are seen to occur at early times, and consequently, Figure 26a presents the same waveforms for a 0.1 ms time window. The corresponding spectral magnitudes are presented in part *b* of the figure. There is about a 20% variation of the peak values of these waveforms.

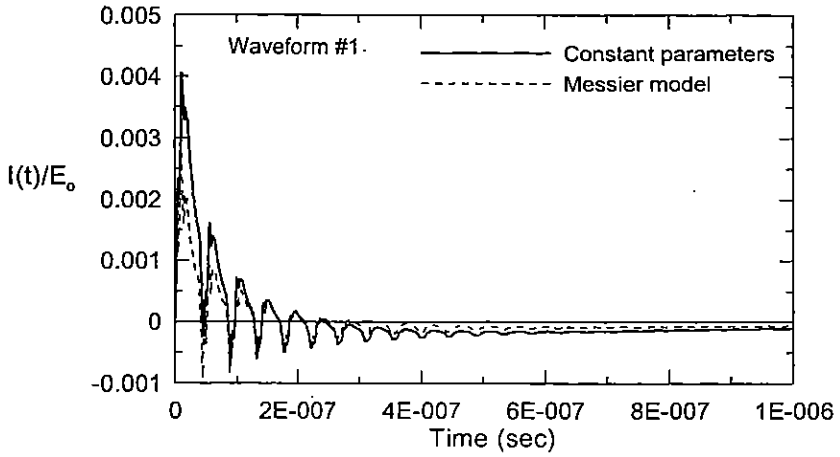

Figure 25. Late-time riser currents for the transmission line of Figure 24, using a constant ground model and the Messier ground model for waveform #1.

Similar plots have been calculated for waveforms #2 and #3, and these are presented in Figure 27 and Figure 28, respectively. As in the case of the reflected and transmitted fields, as the waveform becomes slower, the agreement between the two models improves.

It is evident that the Messier model offers a good solution for the modeling of a lossy earth, as it is based on actual measured data and it provides a causal representation for the parameters. Given this model, it is useful to examine the variations of the computed riser current responses as the model parameters ε_∞ and σ_0.are varied. Using waveform #1, keeping the high frequency dielectric constant fixed at $\varepsilon_\infty = 7.09$, and allowing σ_0.to vary from 0.001 to 0.1 s/m, provides the family of curves and spectral magnitudes presented in Figure 29. Similarly, Figure 30 presents the results obtained by varying the dielectric constant from 1 to 50, with a fixed conductivity of 0.008 s/m.

As noted in these plots., for the fast waveform #1, the variations in the earth conductivity seem to be more important in determining the response of the induced current than do the variations in the dielectric constant. For the slower waveforms, however, the variations in these responses are expected to be less significant.

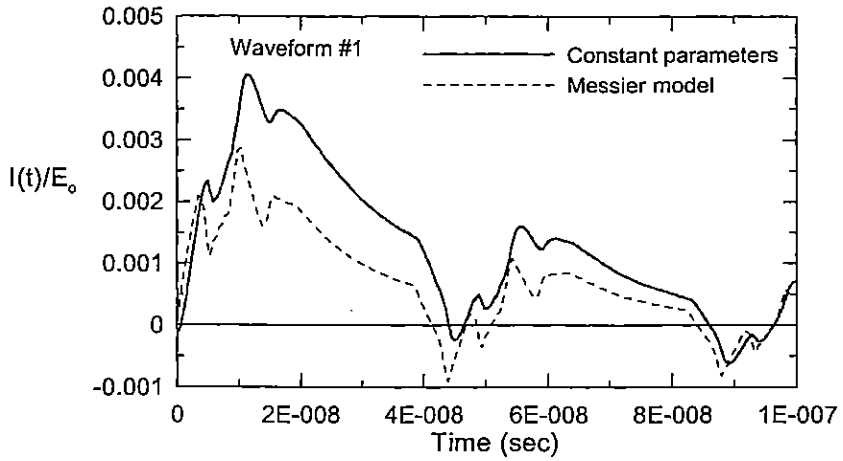

a. Transient responses

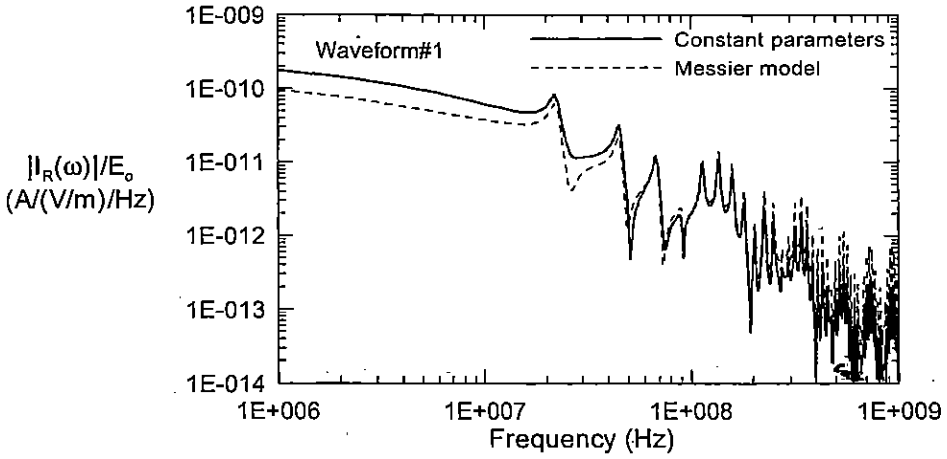

b. Spectral magnitudes

Figure 26. Early-time riser currents (a) and the corresponding spectral magnitudes (b) for the transmission line of Figure 24, using a constant ground model and the Messier ground model for waveform #1.

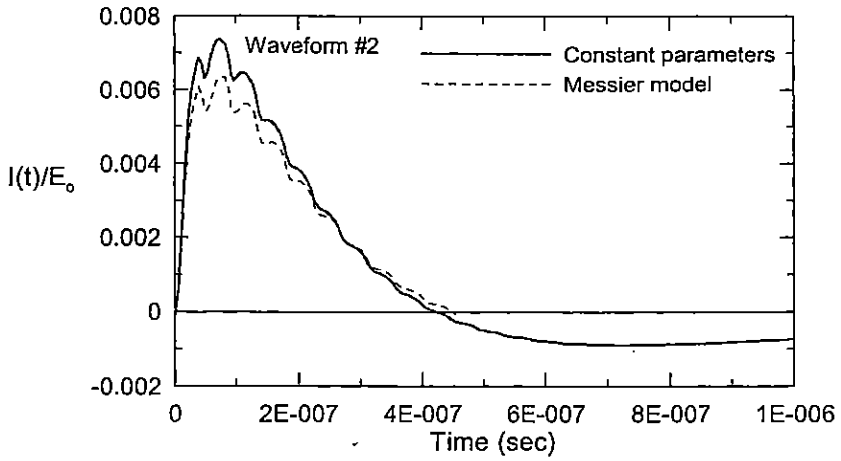

a. Transient responses

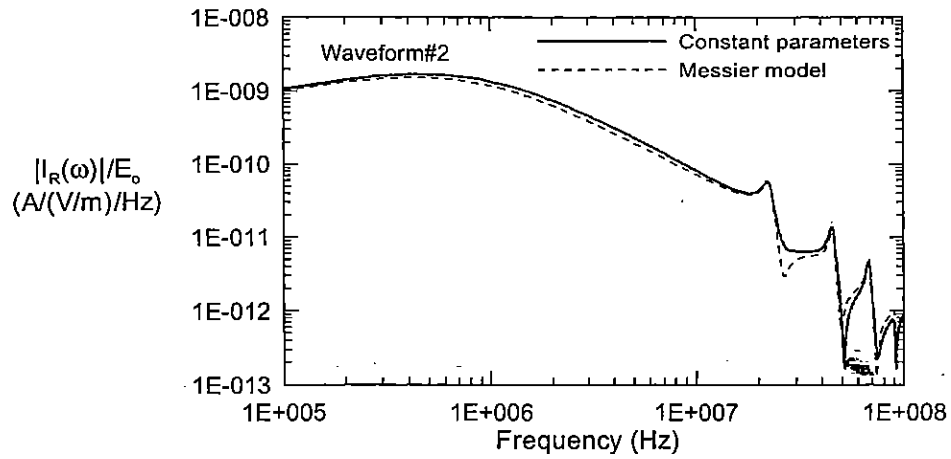

b. Spectral magnitudes

Figure 27. Early-time riser currents (a) and the corresponding spectral magnitudes (b) for the transmission line of Figure 24, using a constant ground model and the Messier ground model for waveform #2.

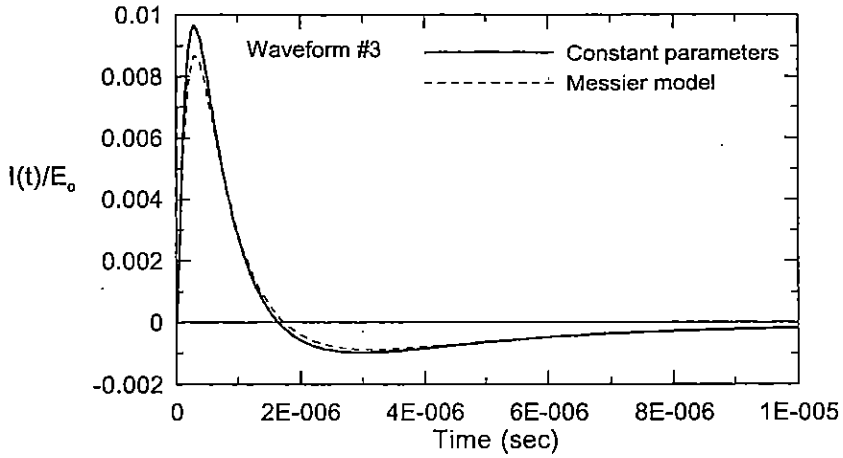

a. Transient responses

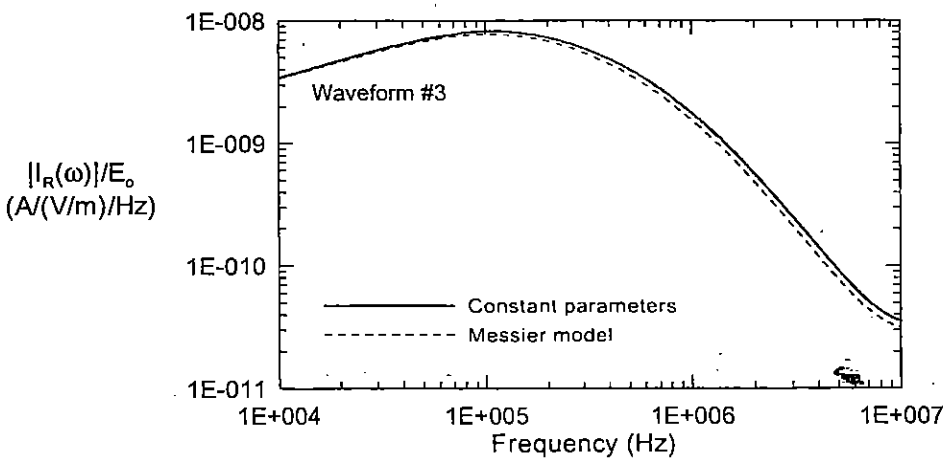

b. Spectral magnitudes

Figure 28. Early-time riser currents (a) and the corresponding spectral magnitudes (b) for the transmission line of Figure 24, using a constant ground model and the Messier ground model for waveform #3.

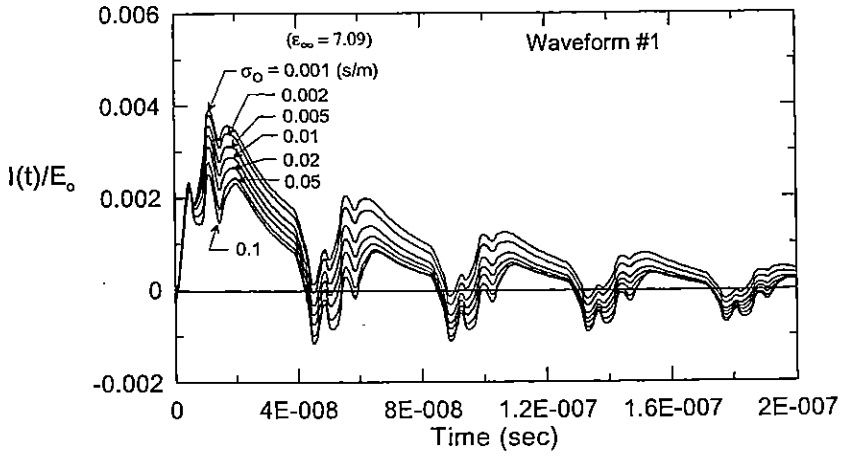

a. Transient responses

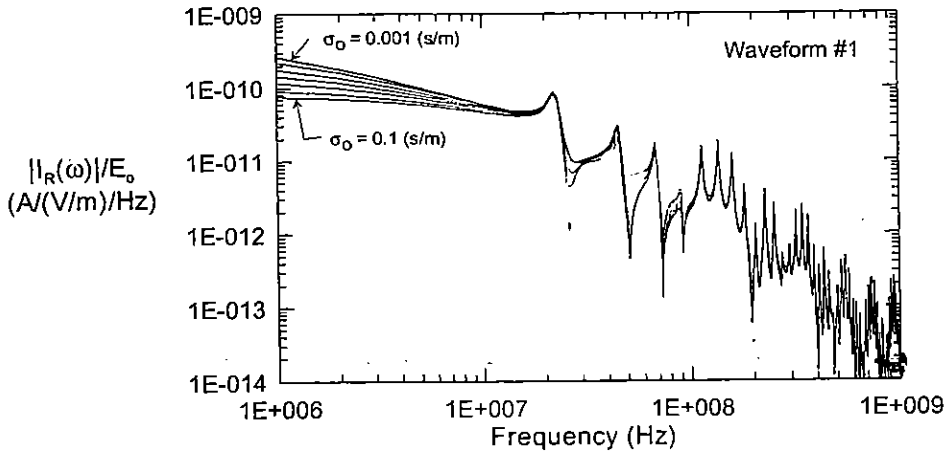

b. Spectral magnitude responses

Figure 29. Sensitivity study of the riser current response using the Messier earth model for variations in the low-frequency conductivity σ_o, keeping the relative dielectric constant fixed at $\varepsilon_\infty = 7.09$.

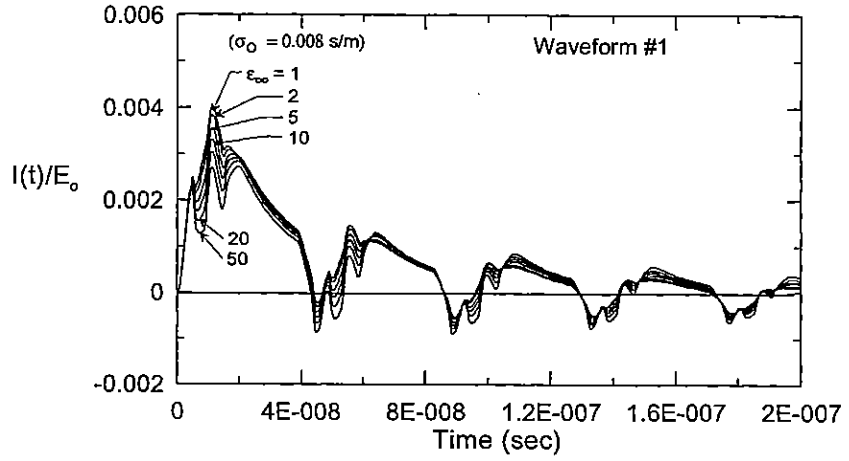

a. Transient responses

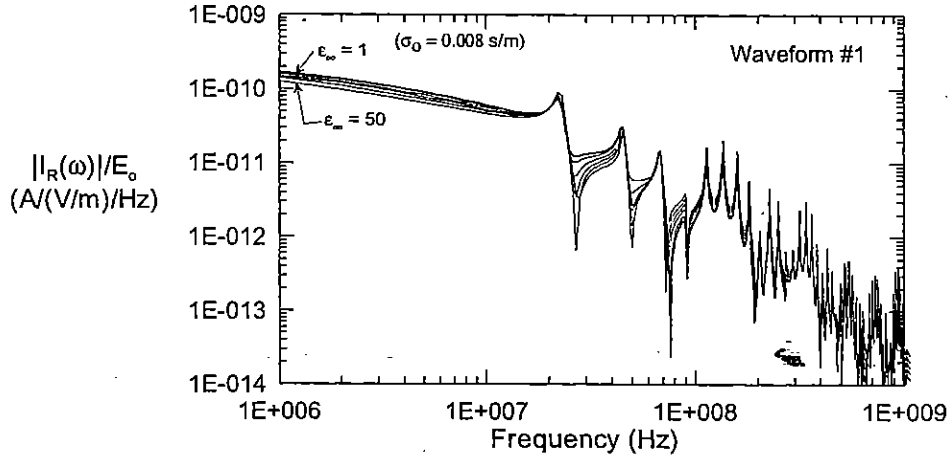

Figure 30. Sensitivity study of the riser current response using the Messier earth model for variations in the relative dielectric constant ε_∞, keeping the low-frequency conductivity fixed at σ_O = 0.008 s/m.

4. Conclusions and Recommendations

This report has investigated the modeling of a lossy earth for transient electromagnetic field calculations. Measurements of the relative dielectric constant and electrical conductivity of the earth indicate that these quantities can vary significantly with frequency, and are not the simple constants that are often used in such calculations. Using several different representations of the frequency dependence of the measured earth parameters, calculations have been performed to illustrate the typical frequency domain and transient behavior of EM fields above and in the earth, as well as the induced currents on an above-ground transmission line.

Three different incident field waveforms have been considered, ranging from a fast 2.93 ns (time to peak) waveform to a slower 29.3 ns waveform. It has been found that for the faster waveform, the field or current responses depend significantly on the particular earth model that is used. However, for the slower waveforms, the differences between the various model results are not as large.

From this study, the following conclusions can be drawn:

1. The frequency dependence of the earth parameters can have a significant effect on EM responses for systems near or in the earth, and thus, this should be incorporated in any EM coupling model.

2. The use of simple measured data, while providing an indication of the frequency variations of the parameters, does not insure causality in calculated responses. This is due to errors in the measured data.

3. Measured data should be fit to causal parameter models, such as the Lorentz or Debye models, to insure causality in any calculated responses.

4. The Messier model for the earth provides a very simple, but causal, two-parameter model for the earth. This has been seen to closely correlate with the results of measured data.

Thus, for future calculations involving lossy earth effects for NEMP or HPM studies, the use of the Messier model is recommended.

5. References

1. Bell Laboratories, *EMP Engineering and Design Principles*, Technical Publications Department, Bell Laboratories, Whippany, NJ. 1975.

2. *EMP Interaction: Principles, Techniques and Reference Data*, K.S.H. Lee, editor, Taylor & Francis Publishing Co. New York, 1989.

3. Tesche, F.M., and P.R. Barnes, "Development of a New High Altitude Electromagnetic Pulse (HEMP) Environment and Resulting Overhead Line Responses," *Electromagnetics*, Vol. 8, No. 2-4, 1988.

4. Ramo, S., J. R. Whinnery and T. Van Duzer, **Fields and Waves in Communication Electronics**, John Wiley & Sons, New York, 1984.

5. Keller, G. V., and F. C. Frischknecht, **Electrical Methods in Geophysical Prospecting**, Pergamon Press, Oxford, 1966.

6. Wait, J. R., **Geo-Electromagnetism**, Academic Press, New York, 1982.

7. Scott, J. H., R. D. Carroll, and D. R. Cunningham, "Dielectric Constant and Electrical Conductivity of Moist Rock from Laboratory Measurements", *Sensor and Simulation Note 116*, Kirtland AFB, NM, August 1964.

8. Scott, J. H., "Electrical and Magnetic Properties of Rock and Soil", *Theoretical Note 18*, Kirtland AFB, NM, May, 1966.

9. Judy, M. M., and W. R. Eberle, "A Laboratory Method for the Measurement of the Dielectric Constant of Rock and Soil Samples in the Frequency Range 10^2 - 10^8 Hertz", *Sensor and Simulation Note 88*, Kirtland AFB, NM, June 1969.

10. Eberle, W. R., "The Effects of Water Content and Water Resistivity on the Dispersion of Resistivity and Dielectric Constant in Quartz Sand in the Frequency Range 10^2 to 10^8 Hz.", *Theoretical Note 82*, August 1970.

11. Bigelow, R. C., and W. R. Eberle, "Empirical Predictive Curves for Resistivity and Dielectric Constant of Earth Materials: 100 Hz to 100 MHz", *Theoretical Note 180*, Kirtland AFB, NM, 1972.

12. Mallon, C. et al, "Low-field Electrical Characteristics of Soil", *Theoretical Note 315*, Kirtland AFB, NM, January 1981.

13. King, R. W. P. (et al), **Antennas in Matter**, MIT Press, Cambridge, Mass., 1981.

14. Baum, C. E., Private communication with the author, June 18, 1999.

15. Longmire, C. L., and H. J. Longley, "Time Domain Treatment of Media with Frequency Dependent Parameters", MRC-N-1, Mission Research Corporation, Santa Barbara, CA, March 1971.

16. Messier, M. A., "The Propagation of an Electromagnetic Impulse Through Soil: Influence of Frequency Dependent Parameters, MRC-N-415, Mission Research Corporation, Santa Barbara, CA, February 1980.

17. Farr, E. G., and C. A. Frost, "Time Domain Measurement of the Dielectric Properties of Water in a Coaxial Test Fixture", *Measurement Note 49*, Kirtland AFB, NM, December 1996.

18. Farr, E. G., and C. A. Frost, "Impulse Propagation Measurements of the Dielectric Properties of Water, Dry Sand, Moist Sand and Concrete", *Measurement Note 52*, Kirtland AFB, NM, November 1997.

19. Tesche, F. M., et al, **EMC Analysis Methods and Computational Models**, John Wiley and Sons, New York, December 1996.

Appendix A

Constitutive Parameters for Lossy Dielectrics and Their Representations in Maxwell's Equations

1. Overview

In many problems in electromagnetics, the effects of a lossy dielectric material are modeled by a scalar permittivity (dielectric constant) ε, a magnetic permeability μ, and a scalar electrical conductivity σ. The fact that these quantities are all frequency independent simplifies considerably the numerical solutions -- both in the frequency domain and in the time domain.

Electrical measurements on some materials, however, indicate that these parameters can vary with frequency. Rock and earth (soil) are examples. For these materials, including this frequency dependence can be important, and if these frequency variations are not included properly, non-causal (unphysical) results can be obtained.

In this appendix, various methods of including this parameter representation in Maxwell's equations are reviewed, and the requirement for having a causal solution is discussed.

2. Time Domain Representation of Maxwell's Equations

Consider first an infinite medium. In the time domain, the behavior of the various electromagnetic field and source quantities are described by the four Maxwell equations [1]

$$\nabla \times \vec{E}(t) = -\frac{\partial \vec{B}(t)}{\partial t} \tag{A1a}$$

$$\nabla \times \vec{H}(t) = \vec{J}_c(t) + \frac{\partial \vec{D}(t)}{\partial t} \tag{A1b}$$

$$\nabla \cdot \vec{D}(t) = \rho(t) \tag{A1c}$$

$$\nabla \cdot \vec{B}(t) = 0 \tag{A1d}$$

where

$\vec{E}(t) =$ Electric field intensity (volts/meter)

$\vec{H}(t) =$ Magnetic field intensity (amperes/meter)

$\vec{D}(t) =$ Electric flux density (coulombs/square meter)

$\vec{B}(t) =$ Magnetic flux density (webers/square meter)

$\vec{J}_c(t) =$ Conduction current density (amperes/square meter)

$\frac{\partial \vec{D}(t)}{\partial t} =$ Displacement current (amperes/square meter)

$\rho(t) =$ Electric charge density (coulombs/cubic meter)

The time variations of these vector and scalar quantities are shown explicitly, and each quantity is also a function of its position in a local coordinate system.

These six quantities are also related by the so-called constitutive parameters:

$$\vec{D}(t) = \overline{\overline{F}}_\epsilon\left(\vec{E}(t)\right) \tag{A2a}$$

$$\vec{B}(t) = \overline{\overline{F}}_\mu\left(\vec{H}(t)\right) \tag{A2b}$$

$$\vec{J}_c(t) = \overline{\overline{F}}_\sigma\left(\vec{E}(t)\right) \tag{A2c}$$

where $\overline{\overline{F}}_\epsilon(\ ), \overline{\overline{F}}_\mu(\ ) and\ \overline{\overline{F}}_\sigma(\ )$ are generalized tensor operators relating the appropriate two transient vector fields. In addition, to these constitutive relationships, there is the equation of continuity [3], which can be derived directly from Eqs.(A1). This expression relates the volume charge density and current density as:

$$\nabla \cdot \vec{J}_c(t) = -\frac{\partial \rho(t)}{\partial t}. \tag{A3}$$

In free-space (vacuum), the tensor operators of Eqs.(A2) are particularly simple, resulting in the scalar constants:

$$\vec{D}(t) = \varepsilon_o \vec{E}(t) \tag{A4a}$$

$$\vec{B}(t) = \mu_o \vec{H}(t) \tag{A4b}$$

$$\vec{J}(t) = 0, \tag{A4c}$$

where $\varepsilon_o = 8.854 \times 10^{-12}$ (farads/meter) is the permittivity of free space (also known as the dielectric constant) and $\mu_o = 4\pi \times 10^{-7}$ (henrys/meter) is the permeability of free space.

The relationships between $\vec{D}(t)$ and $\vec{E}(t)$, $\vec{B}(t)$ and $\vec{H}(t)$ and $\vec{J}_c(t) and\ \vec{E}(t)$ can be extremely complex [2] for a general material. Not only can the material be *anisotropic* (and hence, requiring the tensor relationship), but it also can exhibit a *nonlinear* relationship between the two field strengths. Furthermore, these relationships can be a function of the *past history* of the fields within the material. This latter property leads to the conclusion that the functional dependence between the vector fields in Eqs.(A2) will be expressed in terms of convolution integrals. Thus, the general relationship for the operator in Eq.(A2a) has the form

$$\vec{D}(t)=\int_{-\infty}^{t}\bar{\bar{\varepsilon}}_1(\tau)\vec{E}(t-\tau)d\tau+\int_{-\infty}^{t}\bar{\bar{\varepsilon}}_2(\tau)\vec{E}^2(t-\tau)d\tau+\int_{-\infty}^{t}\bar{\bar{\varepsilon}}_3(\tau)\vec{E}^3(t-\tau)d\tau+\cdots, \qquad \text{(A5)}$$

with similar relationships holding for Eqs.(A2b) and (A2c).

Needless to say, determining the required time dependent tensor quantities to represent a general medium in this manner can be extremely difficult. Consequently, various approximations are usually made for common materials. The most usual approximation is to neglect the possible nonlinear effects in the material[1] and this amounts to eliminating the higher power terms of $\vec{E}$ in Eq.(A5). Furthermore, it is common to neglect the anisotropic behavior of the material in many cases. These approximations permits the relationship between $\vec{D}(t)$ and $\vec{E}(t)$ in Eq.(A5) to take on the simpler form of

$$\vec{D}(t)=\int_{-\infty}^{t}\varepsilon(\tau)\vec{E}(\tau-t)d\tau\,, \qquad \text{(A6)}$$

where $\varepsilon(t)$ is the transient response of the electrical permittivity (i.e., the transient response of the electric flux density $\vec{D}(t)$ for an impulsive electric field $\vec{E}(t)=\vec{\delta}(t)$. Similar relationships again are found for Eqs.(A2b) and (A2c).

As discussed in [2], one possible approximation to the convolution operation in Eq.(A6) is obtained as

$$\vec{D}(t)\approx C_1\vec{E}(t)+C_2\frac{\partial\vec{E}(t)}{\partial t}+C_3\frac{\partial^2\vec{E}(t)}{\partial t^2}+\cdots, \qquad \text{(A7)}$$

where the parameters C_i are constants of the material. Often, only the first two terms in Eq.(A7) are used in this approximation.

This last equation, together with corresponding equations for $\vec{B}(t)$ and $\vec{H}(t)$ and $\vec{J}_c(t)$ *and* $\vec{E}(t)$, form the transient constitutive relationships for the fields within the simplified medium. These relationships and the transient forms of Maxwell's equations in Eq.(A1), are used to determine the electromagnetic fields everywhere within the infinite medium.

As mentioned earlier, the above discussion is valid for a medium of infinite extent. For the case where there is a discontinuity in the medium, such as in the case of an air-earth interface, there are certain other constraints imposed on the behavior of the electromagnetic (EM) fields at the interface [3]. Assuming that there are no external current or charge sources

---

[1] Of course, certain materials, such as $LiNiO_3$, are indeed nonlinear and this behavior may be exploited in optical applications. In these cases, the nonlinear behavior must not be neglected.

impressed at the interface between two different media having a local normal vector denoted as $\hat{n}$, these boundary conditions are given as follows:

$$\hat{n}\times\left(\vec{E}_1-\vec{E}_2\right)=0 \quad \text{(A8a)}$$
$$\hat{n}\times\left(\vec{H}_1-\vec{H}_2\right)=0 \quad \text{(A8b)}$$
$$\hat{n}\cdot\left(\vec{D}_1-\vec{D}_2\right)=0 \quad \text{(A8c)}$$
$$\hat{n}\cdot\left(\vec{B}_1-\vec{B}_2\right)=0\,. \quad \text{(A8d)}$$

If one of the regions is a perfect conductor, say, region 2, the EM fields within this region are identically zero and the boundary conditions become

$$\hat{n}\times\vec{E}_1=0 \quad \text{(A9a)}$$
$$\hat{n}\times\vec{H}_1=\vec{J}_s \quad \text{(A9b)}$$
$$\hat{n}\cdot\vec{D}_1=\rho_s \quad \text{(A9c)}$$
$$\hat{n}\cdot\vec{B}_1=0, \quad \text{(A9d)}$$

where $\vec{J}_s$ and ρ_s are the *surface* current and charge densities existing on the perfectly conducting surface, respectively.

3. Frequency Domain Representation of Maxwell's Equations

Frequently, it is desired to perform field calculations in the frequency domain, where all fields and other responses have the time harmonic representation [4] given by

$$f(t)=\text{Real}[F\,e^{j\omega t}] \quad \text{(A10)}$$

where $f(t)$ is a typical time harmonic response at a frequency $f = \omega/2\pi$ and F is a complex-valued amplitude, called a phasor.

Using this phasor notation and suppressing the exponential functions $e^{j\omega t}$ permits Maxwell's equations to be written in the frequency domain as

$$\nabla\times\vec{E}(\omega)=-j\omega\vec{B}(\omega) \quad \text{(A11a)}$$
$$\nabla\times\vec{H}(\omega)=\vec{J}_{total}(\omega)=\vec{J}_c(\omega)+j\omega\vec{D}(\omega) \quad \text{(A11b)}$$
$$\nabla\cdot\vec{D}(\omega)=\rho(\omega) \quad \text{(A11c)}$$
$$\nabla\cdot\vec{B}(\omega)=0 \quad \text{(A11d)}$$

Where now the fields $\vec{E}(\omega)$, $\vec{H}(\omega)$ etc. are frequency-dependent phasors.

Assuming that only the first two terms in Eq.(A7) (and in the similar expressions for the other constitutive relationships) provide adequate representations for the material responses, the frequency-dependent constitutive parameters for the medium become

$$\begin{aligned}\vec{D}(\omega) &= \left(C_{\varepsilon 1}\vec{E}(\omega) + j\omega C_{\varepsilon 2}\vec{E}(\omega)\right) \\ &= (C_{\varepsilon 1} + j\omega C_{\varepsilon 2})\vec{E}(\omega) \\ &\equiv (\varepsilon' - j\varepsilon'')\vec{E}(\omega) = \varepsilon(\omega)\vec{E}(\omega)\end{aligned} \tag{A12a}$$

$$\begin{aligned}\vec{B}(\omega) &= \left(C_{\mu 1}\vec{H}(\omega) + j\omega C_{\mu 2}\vec{H}(\omega)\right) \\ &\equiv (\mu' - j\mu'')\vec{H}(\omega) = \mu(\omega)\vec{H}(\omega)\end{aligned} \tag{A12b}$$

$$\begin{aligned}\vec{J}_c(\omega) &= \left(C_{\sigma 1}\vec{E}(\omega) + j\omega C_{\sigma 2}\vec{E}(\omega)\right) \\ &\equiv (\sigma' - j\sigma'')\vec{E}(\omega) = \sigma(\omega)\vec{E}(\omega)\end{aligned} \tag{A12c}$$

The six coefficients C_{ij} are typically determined from measurements of the particular material under consideration.

In the expressions in Eqs.(A12), the constitutive parameters μ, ε and σ are frequency-dependent, complex-valued parameters. Considering Eq.(A12a) as an example again, we note that the real part of the dielectric constant is

$$\varepsilon' = C_{\sigma 1}\ , \tag{A13}$$

which is independent of frequency, since $C_{\sigma 1} = C_1$ is a constant in the time domain expression (A7). Furthermore, the imaginary part of the dielectric constant is

$$\varepsilon'' = -\omega C_{\sigma 2}\ , \tag{A14}$$

where $C_{\sigma 2}$ is also a constant. This rather limited functional behavior for the dielectric constant, as well as for the other constitutive parameters in Eq.(A12), is a result of the assumed expansion of Eq.(A7) and our retaining only two terms. More generally, both the real and imaginary parts of the constitutive parameters will be a function of frequency as[2]

$$\varepsilon(\omega) = \varepsilon'(\omega) - j\varepsilon''(\omega) \tag{A15a}$$
$$\mu(\omega) = \mu'(\omega) - j\mu''(\omega) \tag{A15b}$$
$$\sigma(\omega) = \sigma'(\omega) - j\sigma''(\omega). \tag{A15c}$$

---

[2] Traditionally, the negative signs are used in these equations, instead of the positive signs. This is done to insure passivity in the resulting solution for the EM fields within the material.

In the remainder of this development, the explicit frequency dependence of these variables will not be shown.

With the definitions of the constitutive parameters in Eq.(A12), Maxwell's equations in the frequency domain can be written in terms on only the E and H fields and the current and charge sources as

$$\nabla\times\vec{E} = -j\omega\mu\vec{H} \tag{A16a}$$

$$\nabla\times\vec{H} = [\sigma + j\omega\varepsilon]\vec{E} \tag{A16b}$$

$$\nabla\cdot[\varepsilon\vec{E}] = \rho \tag{A16c}$$

$$\nabla\cdot\vec{H} = 0\,. \tag{A16d}$$

In the frequency domain, the charge and current are related by the continuity equation of (A3) as

$$\nabla\cdot\vec{J}_{\epsilon} = -j\omega\rho\,. \tag{A17}$$

As discussed in ref.[5], many materials are non-magnetic, and for these $\mu = \mu' - j\mu'' \approx \mu' \equiv \mu_0$ where μ_0 is the free-space permeability. With this simplification, Eq.(A16a) becomes

$$\nabla\times\vec{E} = -j\omega\mu_{0}\vec{H}\,. \tag{A18}$$

There are several different forms for representing the combined effects of the dielectric constant and electrical conductivity in the curl-H equation of (A16b). Assuming the complex dielectric constant ε and the complex conductivity σ given defined in Eq.(A15), Eq.(A16b) may be written as

$$\nabla\times\vec{H} = [(\sigma' - j\sigma'') + j\omega(\varepsilon' - j\varepsilon'')]\vec{E}\,. \tag{A19}$$

where ε', ε'',σ' and σ'' are all real-valued functions of ω. An alternative form for Eq.(A19) is obtained by collecting real and imaginary parts of the constitutive parameters, as

$$\begin{aligned}\nabla\times\vec{H} &= \left[(\omega\varepsilon'' + \sigma') + j\omega\left(\varepsilon' - \frac{\sigma''}{\omega}\right)\right]\vec{E} \\ &\equiv [\sigma_{eff} + j\omega\varepsilon_{eff}]\vec{E}\end{aligned}\,. \tag{A20}$$

and this expression defines a real-valued, frequency dependent *effective permittivity* and *conductivity* $\varepsilon_{eff}(\omega)$ and $\sigma_{eff}(\omega)$.

In addition to these last two expressions, other forms of this equation are possible by taking various combinations of the real and imaginary parts of the constitutive parameters. These are

$$\begin{aligned}\nabla\times\vec{H} &= [(\omega\varepsilon''+\sigma')+j(\omega\varepsilon'-\sigma'')]\vec{E}\\ &\equiv [\sigma'_{eff}+j\sigma''_{eff}]\vec{E}\\ &= \tilde{\sigma}_{eff}\vec{E}\end{aligned} \qquad \text{(A21)}$$

which defines a complex-valued, frequency-dependent *effective conductivity* $\tilde{\sigma}_{eff}$ of the medium, and

$$\begin{aligned}\nabla\times\vec{H} &= j\omega\left[\left(\varepsilon'-\frac{\sigma''}{\omega}\right)-j\left(\varepsilon''+\frac{\sigma'}{\omega}\right)\right]\vec{E}\\ &\equiv j\omega[\varepsilon'_{eff}-j\varepsilon''_{eff}]\vec{E}\\ &= j\omega\tilde{\varepsilon}_{eff}\vec{E}\end{aligned} \quad , \qquad \text{(A22)}$$

which defines a complex-valued, frequency-dependent *effective dielectric constant* $\tilde{\varepsilon}_{eff}$ of the medium[3].

Finally, using the continuity equation of (A17), the last two divergence equations of Maxwell become

$$\nabla\cdot[\varepsilon_{eff}\vec{E}]=0 \qquad \text{(A23a)}$$

$$\nabla\cdot\vec{H}=0\,. \qquad \text{(A23b)}$$

4. Physical Constraints on the Constitutive Parameters

As pointed out in ref.[2], each of the representations for the constitutive parameters in Eqs.(A19)-(A22) is valid and correct, as these equations are just different arrangements of the fundamental parameters ω, ε', ε'', σ', and σ''. To summarize, the total current (conduction plus displacement) in Eq.(A11b) has the form

$$\vec{J}_{total}=j\omega\hat{\varepsilon}_{eff}\vec{E}=\hat{\sigma}_{eff}\vec{E}=(\sigma_{eff}+j\omega\varepsilon_{eff})\vec{E}=[(\sigma'-j\sigma'')+j\omega(\varepsilon'-j\varepsilon'')]\vec{E}\,. \qquad \text{(A24)}$$

Because of these different ways of representing the behavior of a lossy dielectric, different forms of measured data are reported in the literature, and it is important to realize which parameter is being discussed: $\hat{\varepsilon}_{eff}$, $\hat{\sigma}_{eff}$, σ_{eff}, ε_{eff}, σ', σ', ε' or ε''.

---

[3] Care should be used in distinguishing between the effective complex dielectric constant $\tilde{\varepsilon}_{eff}$ in Eq.(22) and the other real-valued effective dielectric constant ε_{eff} defined in Eq.(20). These are two different quantities. Similarly, the effective complex conductivity $\tilde{\sigma}_{eff}$ Eq(A21) is different from the effective conductivity σ_{eff} in Eq.(A20).

It is useful to note that the above parameters cannot be assigned in an arbitrary matter in any particular medium, as there must be a condition of causality imposed on any solution resulting from Maxwell's equations. By making the assumption that the total polarization field within the material $\vec{P}_{total} = \hat{\varepsilon}_{eff}\vec{E}$ must be a causal function leads directly to the Kramer-Kronig relationships between the real and imaginary parts of the effective complex dielectric constant [5, 6]:

$$\mathrm{Re}\left[\hat{\varepsilon}_{eff}(\omega)\right] = \varepsilon_o + \frac{2}{\pi}\int_0^\infty \frac{\omega' \mathrm{Im}\left[\hat{\varepsilon}_{eff}(\omega')\right]}{\left(\omega'^2 - \omega^2\right)} d\omega' \qquad \text{(A25a)}$$

$$\mathrm{Im}\left[\hat{\varepsilon}_{eff}(\omega)\right] = -\frac{2\omega}{\pi}\int_0^\infty \frac{\left(\mathrm{Re}\left[\hat{\varepsilon}_{eff}(\omega')\right]\right)}{\left(\omega'^2 - \omega^2\right)} d\omega' . \qquad \text{(A25b)}$$

where the integrals must be evaluated as a Cauchy principle values. As discussed in [7 and 8], a slightly more convenient form of these equations is

$$\mathrm{Re}\left[\hat{\varepsilon}_{eff}(\omega)\right] = \varepsilon_o + \frac{2}{\pi}\int_0^\infty \frac{\omega' \mathrm{Im}\left[\hat{\varepsilon}_{eff}(\omega')\right] - \omega \mathrm{Im}\left[\hat{\varepsilon}_{eff}(\omega)\right]}{\left(\omega'^2 - \omega^2\right)} d\omega' \qquad \text{(A26a)}$$

$$\mathrm{Im}\left[\hat{\varepsilon}_{eff}(\omega)\right] = -\frac{2\omega}{\pi}\int_0^\infty \frac{\left(\mathrm{Re}\left[\hat{\varepsilon}_{eff}(\omega')\right] - \mathrm{Re}\left[\hat{\varepsilon}_{eff}(\omega)\right]\right)}{\left(\omega'^2 - \omega^2\right)} d\omega' . \qquad \text{(A26b)}$$

These equations have the same Cauchy principle value as do Eqs.(A25), but the numerator of the integrand vanishes at the singular point $\omega' = \omega$.

Since the effective complex conductivity $\hat{\sigma}_{eff}$ in Eq.(A21) is just the derivative of the effective complex dielectric constant $\hat{\varepsilon}_{eff}$ as $\hat{\sigma}_{eff} = j\omega\hat{\varepsilon}_{eff}$, we note that Eq.(A25) is also valid for the real and imaginary parts of $\hat{\sigma}_{eff}$. Similarly, the σ_{eff} and ε_{eff} parameters of Eq.(A20) are related by the Kramer-Kronig relationships.

These causality relationships form a constraint on any curve-fit representation that may be applied to measured data for dielectric properties of a material. Independent measurements made of σ_{eff} and ε_{eff} over a wide range of frequencies are available for several different types of lossy dielectric material, including the earth. However, many of these measurements do not take into account the requirements of causality. As a consequence, transient results obtained by taking a Fourier transform of a computed spectrum may not be causal.

One way of avoiding this non-causal behavior is to post-process the measured complex dielectric constant using the Kramer-Kronig relationships, as discussed in [8], and illustrated in Figure A1. This involves splitting the complex dielectric constant (denoted by $F_M(\omega)$ in the figure) into its real and imaginary parts, $U_M(\omega)$ and $V_M(\omega)$, respectively. By applying the

Kramer-Kronig relationships (A26) on each and averaging the two resulting complex results provides a filtered causal complex dielectric constant $< F(\omega) >$.

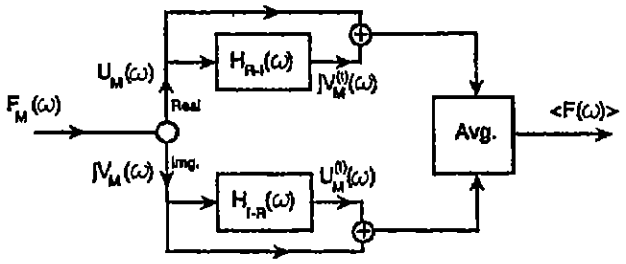

Figure A1. Flow diagram of the causal filtering process.

Alternatively, it is possible to *assume* a functional form for the effective complex dielectric constant $\hat{\varepsilon}_{eff}$ that insures causality, and then fit this model to the measured data for $\sigma_{eff}(\omega)$ and $\varepsilon_{eff}(\omega)$. Two common functional forms that are frequently found in the literature arise from modeling the dielectric by a simple differential equation, known to have a causal solution in the time domain [9]. The Debye model uses the four parameters $\varepsilon_\infty, \varepsilon_s, \tau$ and σ and is of the form

$$\hat{\varepsilon}_{eff} = \varepsilon_\infty + \frac{\varepsilon_s - \varepsilon_\infty}{1 + j\omega\tau} - j\frac{\sigma}{\omega}. \qquad \text{(A27)}$$

In this model, ε_∞ is the high frequency limit of the dielectric constant, ε_s is the low frequency limit of the same, τ is the relaxation time, and σ is the assumed constant static (DC) conductivity.

The Lorentz model takes the form

$$\hat{\varepsilon}_{eff} = \varepsilon_\infty + (\varepsilon_s - \varepsilon_\infty)\frac{(\alpha^2 + \beta^2)}{(\alpha^2 + \beta^2) + j2\omega\alpha - \omega^2} - j\frac{\sigma}{\omega}, \qquad \text{(A28)}$$

with the parameters being $\varepsilon_\infty, \varepsilon_s, \alpha, \beta$ and σ.

As noted in [2], it is possible to consider multiple terms like Eq.(A27) or (A28) to represent the electrical behavior in a complicated dielectric. For example, using the Debye model, a more general representation of the effective dielectric constant would be

$$\hat{\varepsilon}_{eff} = \varepsilon_\infty + \sum_n \frac{f_n}{1 + j\omega\tau_n} - j\frac{\sigma}{\omega}, \qquad \text{(A29)}$$

assuming that there are n terms needed in the sum. A similar sum representation is also possible using the Lorentz model of Eq.(A29) [3].

The finite sum of Eq.(A27) can be also cast into a continuous form, which also provides a causal solution for the effective dielectric constant. This is

$$\hat{\varepsilon}_{eff} = \varepsilon_{\infty} + \int_0^{\infty} \frac{f(\tau)}{1 + j\omega\tau} d\tau - j\frac{\sigma}{\omega}, \tag{30}$$

where $f(\tau)$ is a continuous function that must be evaluated from the measured data.

5. Appendix References

1. Johnk, C. T. A., **Engineering Electromagnetic Fields and Waves**, John Wiley & Sons, New York, 1988.

2. King, R. W. P. (et al), **Antennas in Matter**, MIT Press, Cambridge, Mass., 1981.

3. Balanis, C. A., **Advanced Engineering Electromagnetics**, John Wiley & Sons, New York, 1989.

4. Harrington, R.F., **Time Harmonic Electromagnetic Fields**, McGraw-Hill, New York, 1961.

5. Ramo, S., J. R. Whinnery and T. Van Duzer, **Fields and Waves in Communication Electronics**, John Wiley & Sons, New York, 1984.

6. Jackson, J. D., **Classical Electrodynamics**, John Wiley & Sons, New York, 1975.

7. Guillemin, E. A., **The Mathematics of Circuit Analysis**, MIT Press, 1949

8. Tesche, F. M, "On the Use of the Hilbert Transform for Processing Measured CW Data", *IEEE Trans. EMC,* Vol. 34, No. 3, August 1992.

9. Farr, E. G., and C. A. Frost, "Impulse Propagation Measurements of the Dielectric Properties of Water, Dry Sand, Moist Sand and Concrete", *Measurement Note 52*, Kirtland AFB, NM, November 1997.